AN ABSTRACT OF THE THESIS OF

GANYUAN XIA for the degree of Master of Science in Geophysics presented on June 25, 1993.
Title: Moment-Tensor Inversion for Regional Earthquakes in the Pacific Northwest

Abstract approved: /
John L. Nabelek

With the increasing volume of very broadband digital data available in the Pacific Northwest region, routine data processing techniques become urgent. The moment-tensor inversion method developed in this thesis provides a fast but effective technique for recovering the source mechanism (the moment tensor), the seismic moment, and the source depth by matching the observed waveforms for medium magnitude earthquakes in the Pacific Northwest region. Over time, this will lead to our better understanding of regional tectonic processes here.

Numerical testing performed for frequencies lower than 0.2 Hz shows that the source depth, the seismic moment, and the source orientation are well recovered for three basic types of source mechanisms, 45^0 dip-slip, vertical dip-slip, and horizontal strike-slip. The 45^0 dip-slip has the best depth resolution among the three types, whereas the depth resolution for the strike-slip mechanism is the least good. The inversion depends strongly on an adequately modeled crustal structure for generating Green's functions and depends considerably on an accurate event location. Misalignments between the synthetic and the observed data due to inaccurate determination of epicentral parameters or improper crustal structure can be partly compensated for by appropriate realignments. The source mechanism is relatively

insensitive to the waveform misfit, which proves the robustness of the inversion method.

The inversion technique is applied to three events: the 1993 Scotts Mills event and the 1992 and 1993 Blanco Fracture Zone (BFZ) events. The 1993 Scotts Mills event (m_b=5.6) occurred in the vicinity of the Mt. Angel Fault near Woodburn, Oregon. The inversion of this event was performed in the 0.04-0.1 Hz frequency band and gave a fairly well constrained fault-plane solution: strike=316^0, dip=51^0, slip=162^0, and seismic moment= 2.8×10^{24} dyn cm, corresponding to M_w=5.6, in agreement with m_b=5.6 determined for this event by the International Seismological Center (ISC). The source depth between 10 and 15 km was well constrained. The strike-slip movement is consistent with the strike-slip nature of the Mt. Angel Fault, suggesting that this event could be related to the Mt. Angel Fault.

For the two events from the BFZ, the standard oceanic crustal model was used for generating Green's functions. The epicenters of these two events were not well determined, and were recomputed based on the P-S intervals. The inversion for the 1992 event (m_b=4.8) was done in the 0.01-0.05 Hz band. The inversion yielded a fault-plane solution of strike=211^0, dip=61^0, and slip=290^0, with the slip angle well constrained and the strike and dip angles relatively less constrained. The estimate of seismic moment is about 8.9×10^{23} dyn cm (M_w=5.2). The source depth of 5 km was fairly well constrained. The inversion for the 1993 event (m_b=5.0) was performed in the 0.03-0.05 Hz band, and the solution from the inversion is as follows: strike=122^0, dip=89^0, and slip=38^0 (one fault-plane), $M_0=2.5 \times 10^{24}$ dyn cm (M_w=5.5), depth=5 km. The source depth of 5 km is well constrained. The strike angle has much better resolution than the dip and slip angles. Considering the transform nature of the Blanco Fracture Zone, the 1992 event (normal-fault solution) may have occurred on a fault step over, and the 1993 event (strike-slip solution) directly on the transform boundary.

Moment-Tensor Inversion for Regional Earthquakes in the Pacific Northwest

by

Ganyuan Xia

A THESIS

submitted to

Oregon State University

in partial fulfillment of
the requirement for the
degree of

Master of Science

Completed June 25, 1993

Commencement June 1994

APPROVED:

Redacted for Privacy

Major Professor: Associate Professor of Geophysics

Redacted for Privacy

Dean of College of Oceanic and Atmospheric Sciences

Redacted for Privacy

Dean of Graduate School

Date thesis is presented June 25, 1993

Typed by the author Ganyuan Xia

Acknowledgement

My first thanks should go to my advisor Dr. John Nabelek for his continuous support, his patience and encouragement throughout my graduate study here in OSU.

Thanks should also go to my other committee members: Drs. Gary Egbert, George Moore, and Richard Tubb, who had given me many valuable suggestions and comments.

In addition to my committee members I mentioned above, Drs. John Chen, Bob Duncan, Jack Kenney, Verne Kulm, Shaul Levi, Victor Madsen, Ted Strub, Anne Trehu, and Bob Yeats have contributed to my graduate education. I want to say thanks to you.

Fellow geophysics students during the course of my two and half years graduate study include Ann, Axel, Bird, Christof, Gui-Biao, Jochen, Kelley, Kurt, Luiz, Maureen, Pordur, Soofi, and Xiao-Qing. I would like to thank you for providing me a fine atmosphere to do my research. And I will sure remember our term-Potlucks as well. It always amuses me that many of my fellow students can be an excellent student and a talented cooker in the same time. Special thanks to Steve for helping me get data from Corvallis Station in a much efficient way. Thanks to Gonor, Donna, and Macia for helping me to deal with bureaucratic things.

Dr. George Moore read my thesis draft many times, and helped to polish the manuscript in many ways.

Of course, without the love and prayers of my girl friend Barbara, I might never be able to finish this thesis.

Finally, I would like to thank my parents back in China, they are always supportive.

This work was supported by the U.S. Geological Survey grant 1434-93-G-2326 and the National Science Foundation grant OCE-9203989.

TABLE OF CONTENTS

LIST OF FIGURES

List of Figures (continued)

List of Figures (continued)

LIST OF TABLES

Moment-Tensor Inversion for Regional Earthquakes in the Pacific Northwest

1. Introduction

The Pacific Northwest has typical features of convergent plate boundaries. Deformed Quaternary sediment is found on the continental shelf (Barnard, 1978), a volcanic arc of andesitic composition extends from northern California to southern British Columbia consistent with the presence of a subducting plate beneath the arc, and an interplate Benioff zone has been identified beneath western Washington (Crosson, 1983; Taber and Smith, 1985). But the seismicity in this region shows a rather perplexing pattern (figure 1.1). Compared to the very active seismicity offshore on the transform-fault boundaries, the subduction zone and continental margin of the Pacific Northwest are seismically quiet (Ludwin et al., 1989). The seismicity distribution in the Pacific Northwest contrasts with the global observation where earthquakes occur in both the subducting plate and the overriding plate (Uyeda and Kanamori, 1979).

Based on the hypothesis that the largest earthquakes globally are associated with rapid subduction of young oceanic plates, Heaton and Kanamori (1987) argued that the Casdadia region could sustain a great earthquake of magnitude 8 or larger. Evidence for great Holocene subducting earthquakes was found by Atwater (1987), although the magnitudes and recurrence intervals for those events need further investigation. The recent northern California earthquakes (the Eureka earthquake sequence of April 1992), and the 1993 Scotts Mills earthquake (m_b=5.6) in western

Oregon remind us of the potential for destructive earthquakes in the Pacific Northwest.

The goal of this thesis is to develop an efficient procedure for analyzing earthquake source parameters in the Pacific Northwest region, both onshore and offshore, which will help to improve our understanding of the regional tectonic processes and current stress field.

The techniques for analyzing source processes of large events have been well established over the past decade (e.g., Ward, 1980; Dziewonski et al., 1981; Romanowicz and Guillemant, 1984; Nabelek, 1984). Recently there have been attempts to extend these techniques to analyze medium-magnitude regional events. The most serious problem with regional wave inversion is the inaccurate estimates of Green's functions used for generating synthetic seismograms. In order to deal with this problem, one could go to longer periods for surface-wave inversion (Pasyanos and Romanowicz, 1992; Thio and Kanamori, 1992; Braunmiller et al., 1993), or could fit only portions of seismograms (Dreger and Helmberger, 1993; Randall, 1993). Wallace et al. (1992) compared inversion results of four different inversion techniques for one event, and found that these techniques yielded similar results. Zhao (1993) proposed an alternate approach in which independent Green's functions are used for principal crustal arrivals. In this thesis, a simple but efficient procedure based on matching lower frequency signals is developed.

The basic idea behind determination of a regional source mechanism is rather simple. The observed seismograms are the products of the source effect, the propagation-path effect, and the instrument effect. The instrument effect can be well accounted for and thus removed from the observed seismograms. If the propagation effect is well known, then the source effect can be resolved. The inversion is simply a mathematical approach to this solution.

The inversion code is fully tested using a set of synthesized data. Events from two different regions, Woodburn, Oregon, and the Blanco Fracture Zone are then examined as application examples of this technique. Conclusions and discussion are presented in the last section.

Seismicity of PNW Since 11/89, mb >=3.5

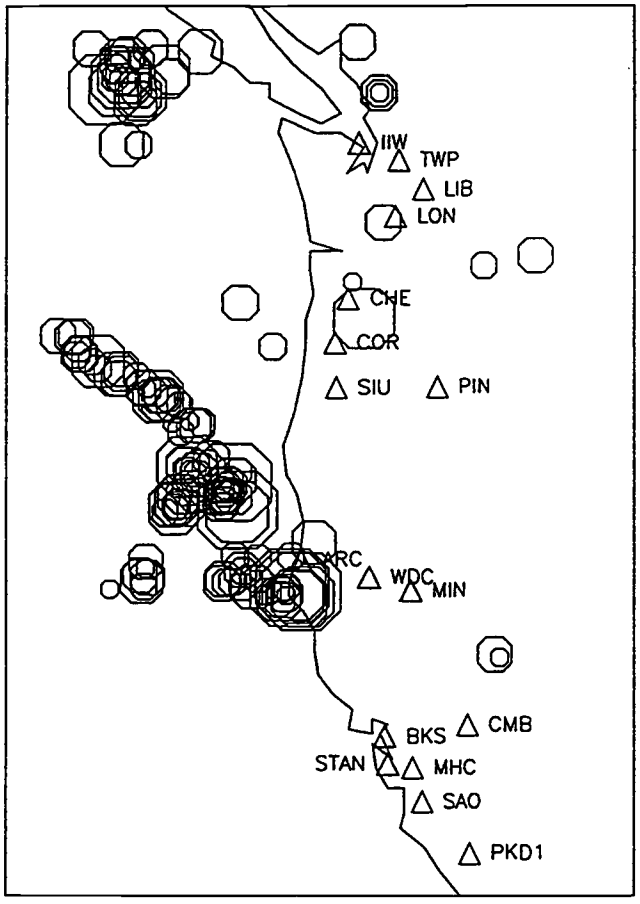

Figure 1.1 Seismicity of the Pacific Northwest since November 1989 for $m_b \geq 3.5$ (data from the preliminary determination of epicenters [PDE] catalogue). Seismic stations are represented by triangles. The most active region is offshore on the transform-fault boundaries; in contrast, the onshore region is seismically quiet.

2. Theoretical Framework

Seismic source can be uniquely expressed by its body-force equivalent (Aki and Richards, 1980), although the physical interpretation of the body-force equivalency is not unique. The seismic moment tensor is a convenient way to describe the physical seismic sources; the zeroth-order moment tensor can be interpreted as a representation of a point source.

The displacement due to the seismic source is the volume integral of the time-domain convolution of Green's function with the seismic moment tensor. For an axially symmetric medium, the Green's function can be separated into P-SV couple and SH components (Wards, 1980), which are conventionally referred to as excitation functions. The displacement field is simply the combination of these excitation functions weighted by the seismic moment-tensor components.

The theoretical part of this thesis is well developed in Nabelek (1984). The following is a brief summary of some of the points needed for formulating both forward and inverse problem in this thesis.

2.1 Forward Problem

2.1.1 Representation of seismic source

For a point impulsive source, the displacement field can be expressed as

$$U^{PSV}(\phi,\Delta,t)=M_n\{I^{PSV^2}(\phi,h,t)\,[\frac{1}{2}(m_{yy}+m_{xx})$$
$$-\frac{1}{2}(m_{yy}-m_{xx})\cos 2\phi+m_{xy}\sin 2\phi]$$
$$+I^{PSV^1}(\phi,h,t)\,[m_{yz}\sin\phi+m_{xz}\cos\phi]$$
$$+I^{PSV^0}(\phi,h,t)\,m_{zz}\}$$
$$U^{SH}(\phi,\Delta,t)=M_n\{I^{SH^2}(\phi,h,t)\,[\frac{1}{2}(m_{yy}+m_{xx})\sin 2\phi+m_{xy}\cos 2\phi]$$
$$+I^{SH^1}(\phi,h,t)\,[m_{yz}\cos\phi-m_{xz}\sin\phi]\}$$

where I^{PSV^0}, I^{PSV^1} and I^{PSV^2} are excitation functions for the P-SV coupled components and I^{SH^1} and I^{SH^2} are excitation functions for the SH component, Δ is the epicentral distance, h is the source centroid depth and ϕ is the station azimuth, m_{xx}, m_{yy}, m_{zz}, m_{xy}, m_{xz}, and m_{yz} are normalized moment-tensor elements, M_n is the moment-tensor norm, the first invariant of the moment tensor. For a double-couple source, the seismic moment M_0 is

$$M_0=\frac{1}{\sqrt{2}}M_n$$

2.1.2 Computation of excitation functions

The method for computing excitation functions is the discrete wavenumber summation technique proposed by Bouchon (1981,1982). This technique produces completed synthetic seismograms for horizontally layered structures and allows for inelastic attenuation.

2.1.3 Source parameterization

Source parameterization is the key to any inverse problem. Overparameterization will cause a tradeoff among model parameters. Oversimplified parameterization will obviously lead to inadequate description of the model. Since we are dealing with regional earthquakes of medium magnitude, our model parameters become relatively simple. At sufficiently long periods, the source can be treated as a point source, therefore only the moment tensor and source time function need to be considered.

Following Nabelek (1984), the source time function $\Omega(t)$ is parameterized as overlapping isosceles triangles with the form

$$\Omega(t)=\sum_{k} w_k T_{\Delta\tau}(t-\tau_k)$$

$$T_{\Delta\tau}(t)=B_{\Delta\tau}(t)*B_{\Delta\tau}(t)$$

$$\tau_k=\Delta\tau(k-1)$$

where $B_{\Delta\tau}(t)$ is the box function. Amplitudes w_k are determined by the inversion, but the number of triangle elements and their durations are chosen *a priori*.

Source depth is a model parameter not directly determined from inversion, inasmuch as excitation functions for different depths are not a simple combination or delayed summation of some elementary seismograms; rather, source depth is determined from locating the minimum in a variance vs depth plot.

2.1.4 Forward problem

The synthetic seismogram can be written in the form

$$s(t)=M_n \sum_{k=1}^{n} \sum_{i=1}^{m} w_k H_i(t-\tau_k) r_i$$

where $H_i(t)=h_i(t)*T_{\Delta\tau}(t)$, and

M_n - moment-tensor norm
w_k - weight of the source time function element k
$H_i(t)$ - elementary seismogram
t - time
τ_k - time shift of a time-function element
r_i - normalized source-radiation pattern
n - number of source time function elements
m - 6 for P-SV waves and 4 for SH waves
$h_i(t)$ - excitation functions produced by a step source
$T_{\Delta\tau}(t)$ - normalized time-function element.

The whole seismogram is constructed by a weighted and time-shifted sum of the elementary seismograms $H_i(t)$. As long as the source position is fixed, the excitation functions $h_i(t)$ can be stored, and new seismograms of any source orientation and time function can be computed efficiently.

2.2 Inverse Problem

2.2.1 Least-squares inversion

Our goal is to retrieve source information from matching the observed data-bearing source signatures with the synthetics (our model prediction). Many uncertainties affect an ideal match, such as, seismic noise, complex structures, and complex source. Therefore, the objective function is established that takes the square of residuals between the synthetic and observed data. The source information is recovered by minimizing the residuals.

If the data and model parameters follow Gaussian statistics, L_2 norm inversion is performed, which is essentially a least-squares inversion (Tarantola and Valette, 1982; Menke, 1984). The objective function is

$$\chi^2=[\underline{d}-\underline{m}(\underline{P})]^T\underline{C}_{d_0}^{-1}[\underline{d}-\underline{m}(\underline{P})]+[\underline{P}_0-\underline{P}]^T\underline{C}_{p_0}^{-1}[\underline{P}_0-\underline{P}]$$

where $\underline{d}$ is the observed seismogram, $\underline{m}$ is the synthetic seismogram, $\underline{P}$ represents model parameters, $\underline{C}_{d_0}$ is the covariance of data, and $\underline{C}_{p_0}$ is covariance of model parameters.

The minimum of the above expression is found iteratively. The improvement from the *k*th to *k+1*th iteration can be expressed as (Nabelek, 1984)

$$\underline{P}_{k+1}=\underline{P}_k+[\underline{A}_k^T\underline{A}_k+\varepsilon_0\underline{I}]^{-1}[\underline{A}_k^T\underline{f}_k]$$

$$\underline{A}_k=\begin{bmatrix}\underline{C}_{d_0}^{-\frac{1}{2}}\underline{J}_k\\ \underline{C}_{p_0}^{-\frac{1}{2}}\end{bmatrix}$$

$$\underline{f}_k=\begin{bmatrix} \underline{C}_{d_0}^{-\frac{1}{2}}\,(\underline{d}-\underline{m}(\underline{P}_k)) \\ \underline{C}_{p_0}^{-\frac{1}{2}}\,(\underline{P}_0-\underline{P}_k) \end{bmatrix}$$

where A_k is the Jacobian

$$A_{ij}=\frac{\partial m_i}{\partial P_i},$$

ε_0 is the damping factor introduced to stabilize the inversion, and $\underline{I}$ is a unit diagonal matrix.

In most cases we have no *a priori* information about source parameters. This means

$$\underline{C}_{p_0} \rightarrow \infty.$$

The algorithm for solving the least-squares problem is taken from Lawson and Hanson (1974) with a positivity constraint on the source time function.

2.2.2 Computation of partial derivatives

The Jacobian A_{ij} can be explicitly expressed as follows

$$\frac{\partial U^{PSV}}{\partial am_1} = I^{PSV^2}\cos 2\phi$$

$$\frac{\partial U^{PSV}}{\partial am_2} = I^{PSV^2} \sin 2\phi$$

$$\frac{\partial U^{PSV}}{\partial am_3} = I^{PSV^1} \cos\phi$$

$$\frac{\partial U^{PSV}}{\partial am_4} = I^{PSV^1} \sin\phi$$

$$\frac{\partial U^{PSV}}{\partial am_5} = I^{PSV^0}$$

$$\frac{\partial U^{PSV}}{\partial am_6} = I^{PSV^2}$$

$$\frac{\partial U^{SH}}{\partial am_1} = -I^{SH^2} \sin 2\phi$$

$$\frac{\partial U^{SH}}{\partial am_2} = I^{SH^2} \cos 2\phi$$

$$\frac{\partial U^{SH}}{\partial am_3} = -I^{SH^1} \sin\phi$$

$$\frac{\partial U^{SH}}{\partial am_4} = I^{SH^1} \cos\phi$$

where

$$am_1 = \frac{1}{2}(m_{xx} - m_{yy})$$

$$am_2 = m_{xy}$$

$$am_3 = m_{xz}$$

$$am_4 = m_{yz}$$

$$am_5 = m_{zz}$$

$$am_6 = \frac{1}{2}(m_{xx} + m_{yy})$$

As we can see from the above expression, the partial derivatives are simple weighted sums of excitation functions. This makes an efficient inversion possible.

2.2.3 Noise consideration

Since the inversion is minimizing L_2 norm of the residuals between the synthetic and observed data, random Gaussian noise does not bias the inversion results. But signal-generated noise, such as noise signals from strong heterogeneous reflectors, will cause serious problems to the inversion and therefore needs special attention. Other factors affecting an ideal match include unmodeled structure used for generating synthetic data, mislocation of events, etc.

2.3 Practical Considerations

2.3.1 Geometric spreading

To correct for the geometric spreading effect, two types of normalization are applied to the data depending on the station's epicentral distance. The r/r_n type (body-wave type) is used for the close stations, and the $\sqrt{r}/\sqrt{r_n}$ type (surface-wave type) is for the farther stations, where r is the epicentral distance of the station and r_n is the normalization distance. The same type of normalization has to be applied to the corresponding synthetic seismograms.

2.3.2 Interactive processing

The inversion code was written as an interactive program. Generally, once the model parameters are determined by the inversion, one has to go back to see if the matches

between the model prediction and the observation are acceptable. If not, one can further filter the data or increase model parameters or apply certain constraints on the model. If any phase shifts are present between the data and the synthetics, one can apply realignment, seeking the maximum of the cross correlation between the data and the synthetics. For a given station, the realignment shifts the synthetic seismograms of all components by the same amount, and different stations can have different time shifts. This process can go on until an acceptable model is reached.

2.3.3 Stability of the inversion

Techniques used in this thesis to stabilize inversion are:

1) applying firm bounds on parameters based on physical considerations (e.g. requiring a positive source time function),

2) low-pass filtering the model by damping the small eigenvalues (especially useful for an overparameterized model, usually source time functions),

3) forcing firm relations between certain parameters (e.g. a deviatoric constraint on the moment tensor),

4) varying duration of the source time function elements,

5) fixing unresolved parameters.

3. Testing with Synthetic Data

In order to investigate the resolving power of the regional-wave-inversion method to recover the source mechanism and source time history, a set of synthetic data with known source parameters is constructed to form the "observed" data for the testing.

3.1 "Observed" Data Preparation

A set of synthetic data is generated for four imaginary stations STA1, STA2, STA3, and STA4. The station parameters are summarized in Table 1. The four stations are distributed asymmetrically around the source, with epicentral distance ranging from 75 km to 300 km. The source has only one triangular time function with a 2-second duration, and the seismic moment is 1.0×10^{24} dyn cm. To give equal weight to each station, two different time windows and corresponding sampling periods are used for the four stations according to the station epicentral distance, specifically, 64 seconds with a 0.125-second sampling period for STA2 and STA4 and 128 seconds and with a 0.25-second sampling period for STA1 and STA3.

All the following tests are performed at frequencies lower than 0.2 Hz except when stated explicitly, the surface-wave type of normalization is applied to both the data and the synthetics, and the inversion results are summarized in Table 2.

3.2 Depth Resolution

Three types of source mechanisms, namely, 45^0 dip-slip, vertical dip-slip, and horizontal strike-slip are tested, with the same structure as the one used for constructing the imaginary "observed" data and the same source depth of 15 km. These three orientations are responsible for generating three excitation functions I^0, I^1 and I^2, and are thus chosen for our testing purposes. Four overlapping triangular source time functions, each with 1 second half-duration are included in the model parameters. For all three types, seismic moment, source time function, and source orientation are recovered from the inversion. Normalized variance vs depth plots gives a well defined source depth of 15 km for all three source orientations (figure 3.1). The 45^0 dip-slip source has the best depth resolution in this group, and the strike-slip source the worst.

3.3 Sensitivity to Crustal Structure

Three different crustal models are introduced for all four imaginary stations to explore the sensitivity of the inversion to crustal structure. I use the 45^0 dip-slip as the targeting source orientation.

The first variation is to increase P wave velocities by 5% and 10% everywhere. Fixing the Possion ratio at 0.25, the S wave velocities and densities are computed accordingly. Figure 3.2a shows the waveform match for the 10% velocity increase without realignment. The time shifts between the data and the synthetics are quite obvious. Therefore, realignment between the synthetics and the data was then performed (figure 3.2b). After the realignment, the surface waves are matched very well, however, the P waves are coming

too late for the two more distant stations (STA1 and STA3), due to less time difference between P and S arrivals (figure 3.2a). Estimates of the strike and slip angles from the inversion are off by about 5^0 (see Table 2). For the case where velocity increases by 5% and proper realignment is allowed, both P and S waves are well matched (figure 3.2c). Inversion gives a source orientation of strike=44.9^0, dip=44.9^0 and slip=90.4^0 with seismic moment of 1.32×10^{24} dyn cm. The source mechanism is perfectly recovered. Considering the higher average velocity structure, the slightly higher estimate of seismic moment is comprehensible. So a 5% velocity increase may be the largest average velocity variation that can be tolerated for this test case. This is not a universal conclusion; the effect of velocity variation depends on the epicentral distance and the frequency band.

Next we investigate the effect of the top layer. Keeping the Moho depth fixed, the thickness of the top layer is increased by 1 km and 3 km, respectively. Again, realignment between the data and the synthetics is allowed to correct for arrival-time discrepancies. As shown in figure 3.3a for the case of a 3-km thickness increase, the synthetics have more surface waves, which are not seen in the data because surface waves are more developed in a much thicker top layer. The inversion yields a source orientation of strike=38.3^0, dip=42.9^0, and slip=79.4^0 with a seismic moment of 0.82×10^{24} dyn cm; the strike and slip angles are strongly biased. One could expect that a better estimation of source parameters could be obtained by inverting for longer period waves. Figure 3.3b shows the waveform match for frequencies lower than 0.05 Hz. The Rayleigh waves are slightly more dispersed, but the source mechanism is almost fully recovered (strike=44.9^0, dip=44.7^0, and slip=90.4^0). The thickening of the top layer pushes the effective source down. Shown in figure 3.3c is the variance plotted as a function of source depth from the inversion for frequencies

lower than 0.05 Hz. The effective source depth changed to 16 km.

If the thickness increase of the top layer is only 1 km, the frequency content of both the data and the synthetics is similar (figure 3.3d), the waveform match is reasonably good, although a slight difference can still be observed, especially at transverse components of STA1 and STA3. The estimate of source mechanism is not improved much except for the slip angle, but the seismic moment estimate is more accurate (1.01×10^{24} dyn cm) because of the improved fit between the synthetics and the data. Similarly, inversion for frequencies lower than 0.05 Hz recovers the source mechanism (strike=45.7^0, dip=44.9^0 and slip=90.7^0) (figure 3.3e).

The third variation is to move the Moho up by 5 km; in general, the synthetics fit the data very well (figure 3.4).

Clearly the inversion strongly depends on the average velocity structure and also the shallow structure, whereas it doesn't depend much on deeper structure. This is probably due to the fact that we are mainly inverting for lower frequency regional surface waves, which are not sensitive to deeper structures at this frequency range. The effect of the top layer decreases as the inverting frequencies go lower, because the relatively thin top layer becomes transparent to longer period waves. If source-mechanism bias on the order of 5^0 is acceptable, the above tests show that very precise knowledge of the crustal structure is not neccessary for inversion of frequencies below 0.2 Hz.

3.4 Mislocation Test

If the origin time or the location of an event are not well determined, a straightforward inversion will lead to biased estimates of source parameters, or in the worst

situation, totally wrong solutions. To simulate this kind of situation, misdetermined origin time and epicenter are artificially introduced in the testing.

The first example is the same 45^0 dip-slip event with an origin time determined 5 seconds earlier. The waveform match is messy (figure 3.5a); for example, polarities of some of the traces are opposite. If eight triangles are allowed to play in the inversion, however, the source parameters are recovered, and the waveform matches are nearly perfect (figure 3.5b). Notice that now the source time function starts about 5 seconds later after the misdetermined origin time and has about a 2-second duration, which is exactly what the source process should be. It seems that a proper longer source time function can correct for a too-early origin time.

For the same event with an origin time determined 5 seconds late, a straightforward inversion does not work at all. As shown in figure 3.6a, the synthetics do not resemble the data in general waveforms. Further complication of source time functions won't be able to help solve this problem. In this case, proper realignments that maximize the cross correlation between the synthetics and the observed data can overcome the problem. Figure 3.6b shows the waveform match after the realignment; the match is then perfect. The realignment amount of 5 seconds exactly corrects for the 5 second discrepancy.

A misdetermined origin time imposes no serious problem, because it's a one-way time shift for all stations and does not affect the Green's functions. But a mislocated epicenter does. Mislocation leads to biased estimates of both epicentral distance and station azimuth. It's mainly the misdetermination of epicentral distance that causes biased estimates of the Green's functions, which cannot be compensated for by the realignment. To see how far off is considered unacceptable, the epicenter is moved due north by 5 km and 10 km, respectively. The inversion shows that the 10 km epicenter mislocation can make a considerable

difference to the match of waveforms, especially for the closer stations (figure 3.7a). As shown in figure 3.7a, both the amplitude and phase of the radial component of STA2, which is the closest station, is not well matched. A satisfactory match can be reached only at 5 km off (figure 3.7b). The inversion results are listed in table 2.

3.5 Summary and Discussion

Source parameters are all recovered for three basic source orientations (45^0 dip-slip, vertical dip-slip, and horizontal strike-slip). The source depth is well resolved by minimizing the variance. The inversion method strongly depends on the shallow crustal structure but not on the deep structure. The thickening of the top layer results in a deeper effective source. Misdetermined origin time can be corrected by either applying appropriate source time functions or by performing proper realignments. The inversion relies considerably on an accurate epicenter location.

In general, the seismic moment is more sensitive to any phase misfit than to any other parameters. The source mechanism, on the other hand, is relatively insensitive to errors in the earth model or assumed source depth. At sufficiently low frequency , adequate phasing can be achieved, and the inversion can give good estimates of both the seismic moment and the source mechanism.

Table 1. Station parameters for the synthetic data set, and the velocity structure used for generating the synthesized "real" data.

Station	Azimuth (^{0})	Δ (km)
STA1	20.0	300.0
STA2	160.0	75.0
STA3	250.0	200.0
STA4	280.0	100.0

Velocity structure

Depth (km)	Vp (km/s)	Vs (km/s)	ρ (g/cm^3)
2.0	4.00	2.14	2.14
35.0	6.50	3.75	2.84
∞	8.10	4.68	3.29

Table 2. Summary of inversion results for the test data.

Test type	strike (^{0})	dip (^{0})	slip (^{0})	moment (10^{24} dyn cm)
45^0 dip slip	45.4	45.0	90.5	0.972
vertical dip slip	0.0	89.6	90.0	0.975
vertical strike slip	0.0	90.0	0.0	0.978
velocities increase by 10%	26.7	53.9	67.2	1.11
after realignment	40.7	45.4	85.2	1.66
velocities increase by 5%	47.3	50.9	102.1	1.18
after realignment	44.9	44.9	90.4	1.32
thickness of top layer increases by 3 km	76.9	50.9	125.7	0.239
after realignment	38.3	42.9	79.4	0.820
inversion for f < 0.05 Hz	42.0	41.7	89.1	0.825
after realignment	44.9	44.7	90.4	0.845

Table 2. (continued)

thickness of top layer increases by 1 km	51.1	41.4	98.5	0.690
after realignment	39.5	42.7	83.3	0.983
inversion for f < 0.05 Hz	45.1	44.0	90.4	0.955
after realignment	45.7	44.9	90.7	0.951
Moho shifted up by 5 km	47.5	45.2	93.0	1.01
origin time determined 5 s earlier	44.6	40.1	287.6	0.933
after source time function correction	45.0	45.0	89.9	1.03
origin time determined 5 s later	48.3	47.4	275.2	0.513
after realignment	45.3	45.0	90.5	0.967
epicenter shifted north by 10 km	51.5	39.9	38.5	0.641
after realignment	48.5	49.4	95.3	1.02
eicenter shifted north by 5 km	58.8	58.6	108.7	0.870
after realignment	49.2	47.9	95.5	0.998

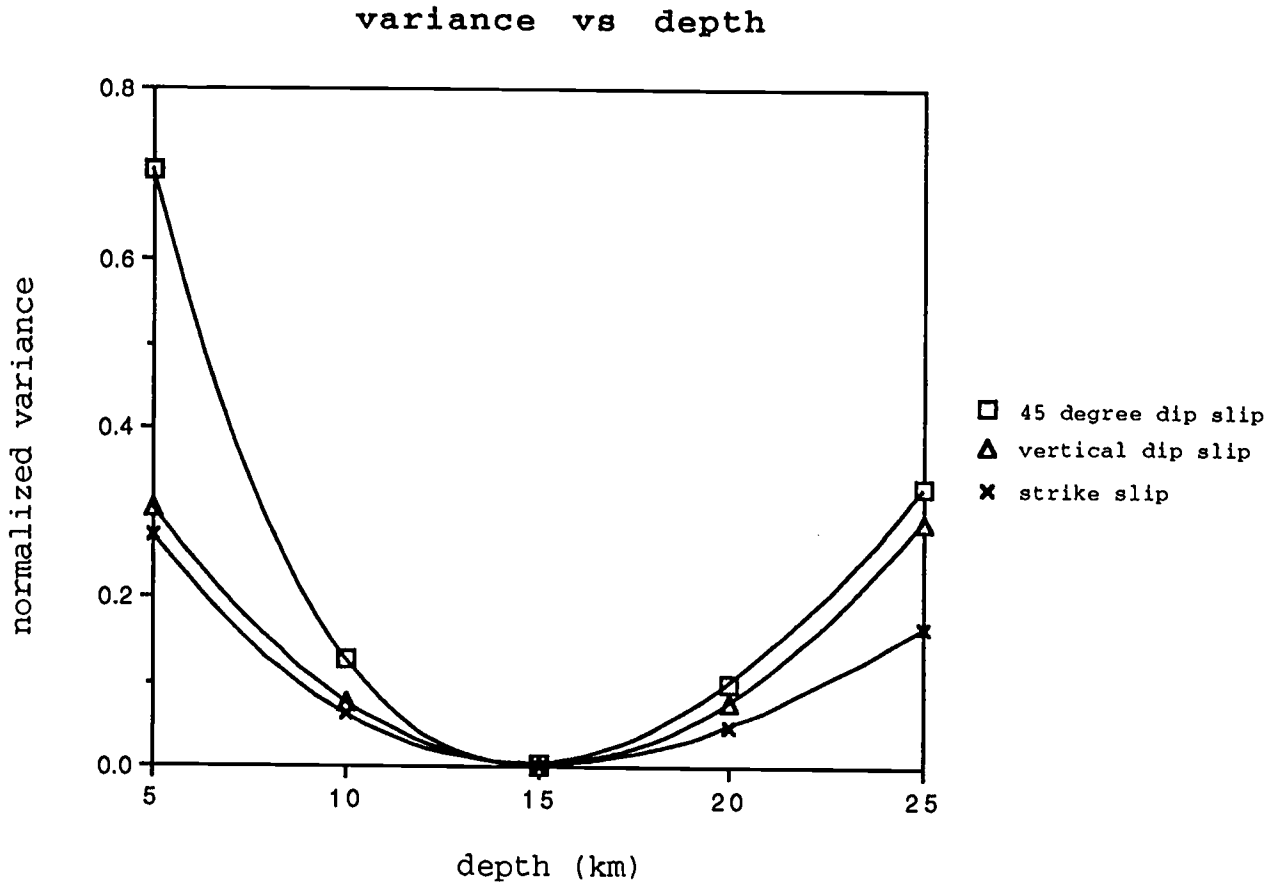

Figure 3.1 Normalized variance versus source depth showing a well defined source depth at 15 km for three types of source orientation (45^0 dip-slip, vertical-dip slip, and horizontal strike-slip). The 45^0 dip-slip source mechanism has a slightly better depth resolution.

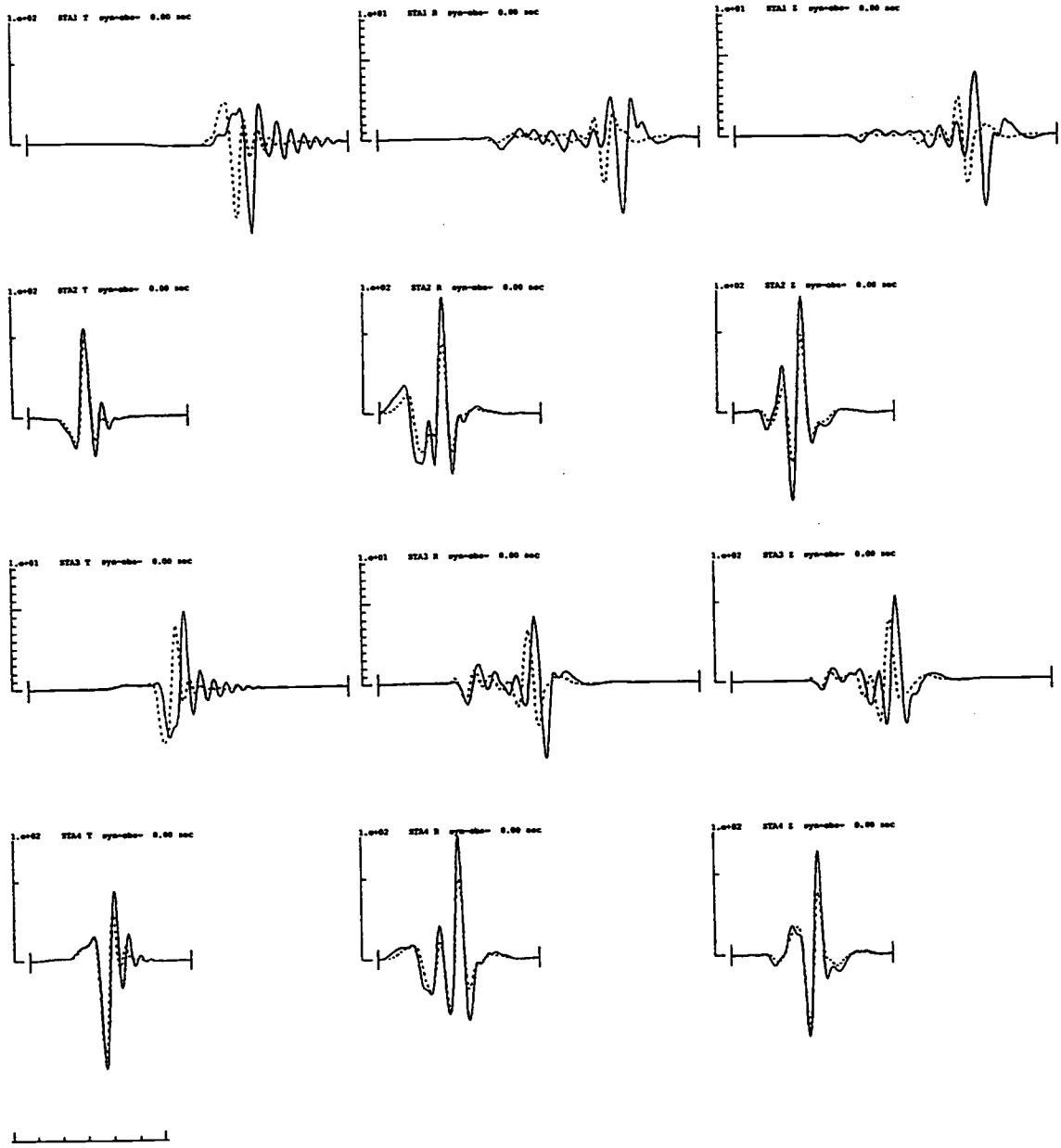

Figure 3.2a Sensitivity of the inversion to crustal structure-case I: velocities increase by 10% everywhere. The solid lines are for the data and the dash lines for the synthetics. Traces from top to bottom are for stations, STA1, STA2, STA3, and STA4. Traces from left to right are for transverse, radial, and vertical components, respectively.

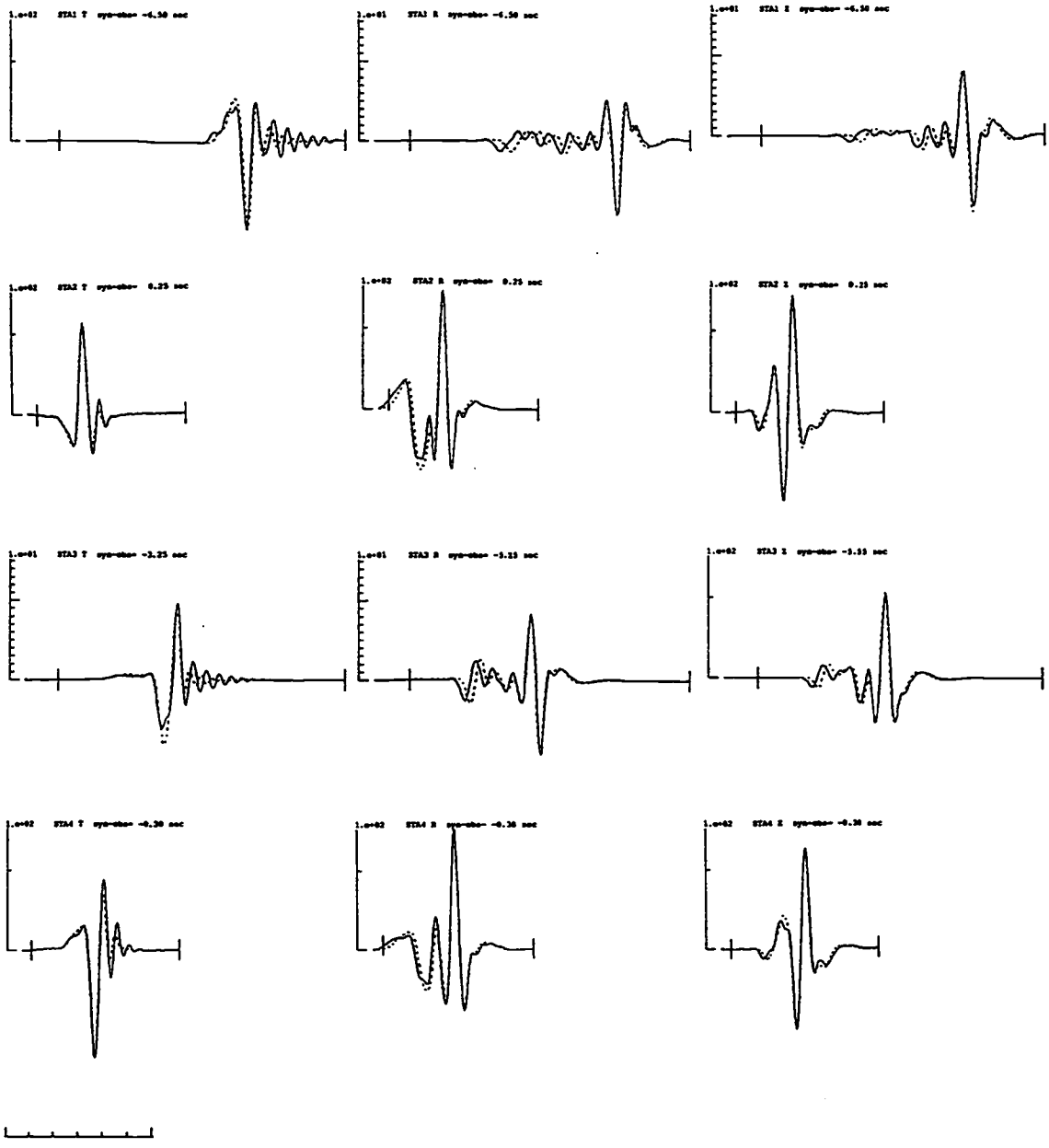

Figure 3.2b Same as figure 3.2a, except realignment is allowed.

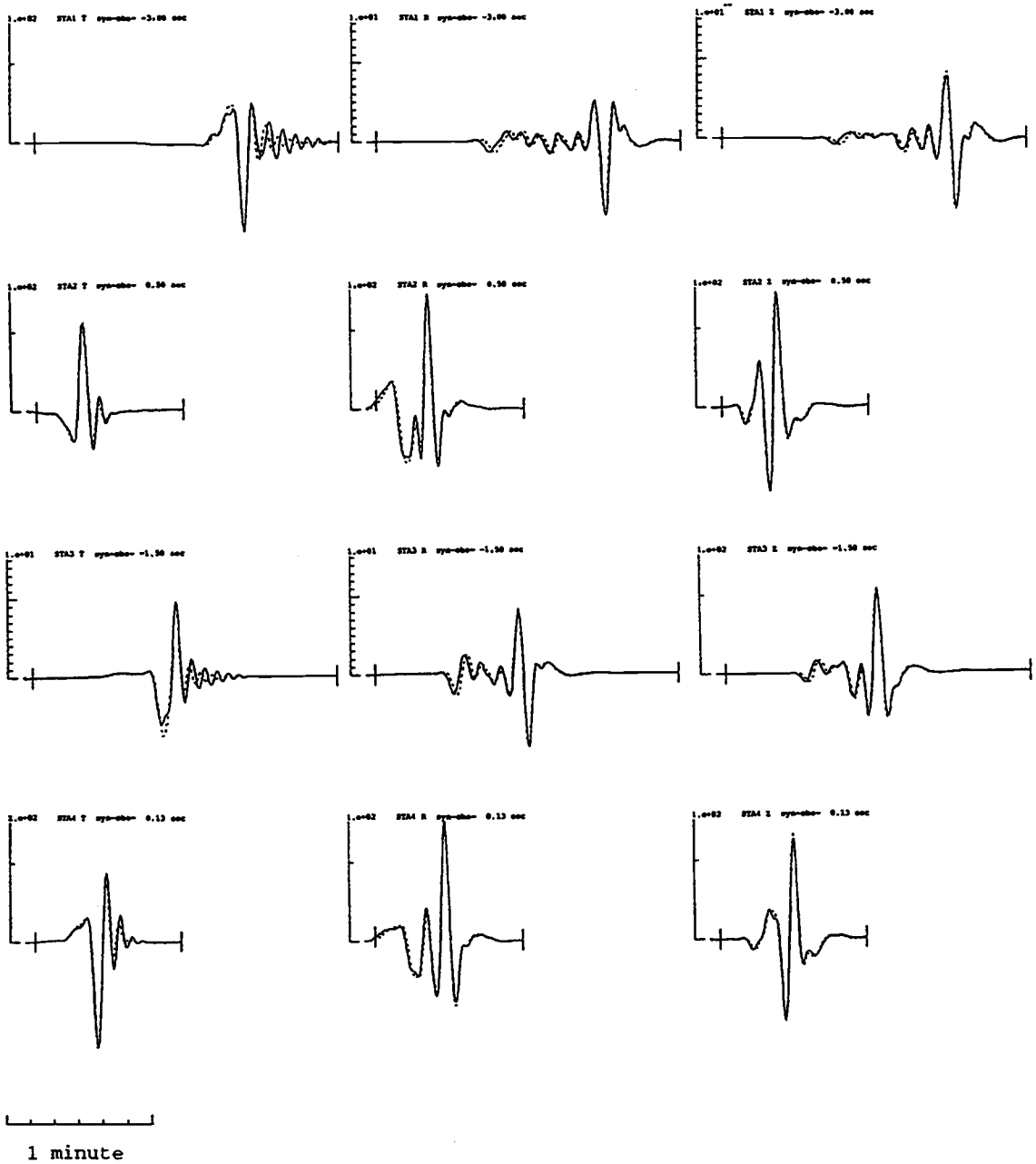

Figure 3.2c Same as figure 3.2a, except for 5% velocity increase, and realignment is allowed.

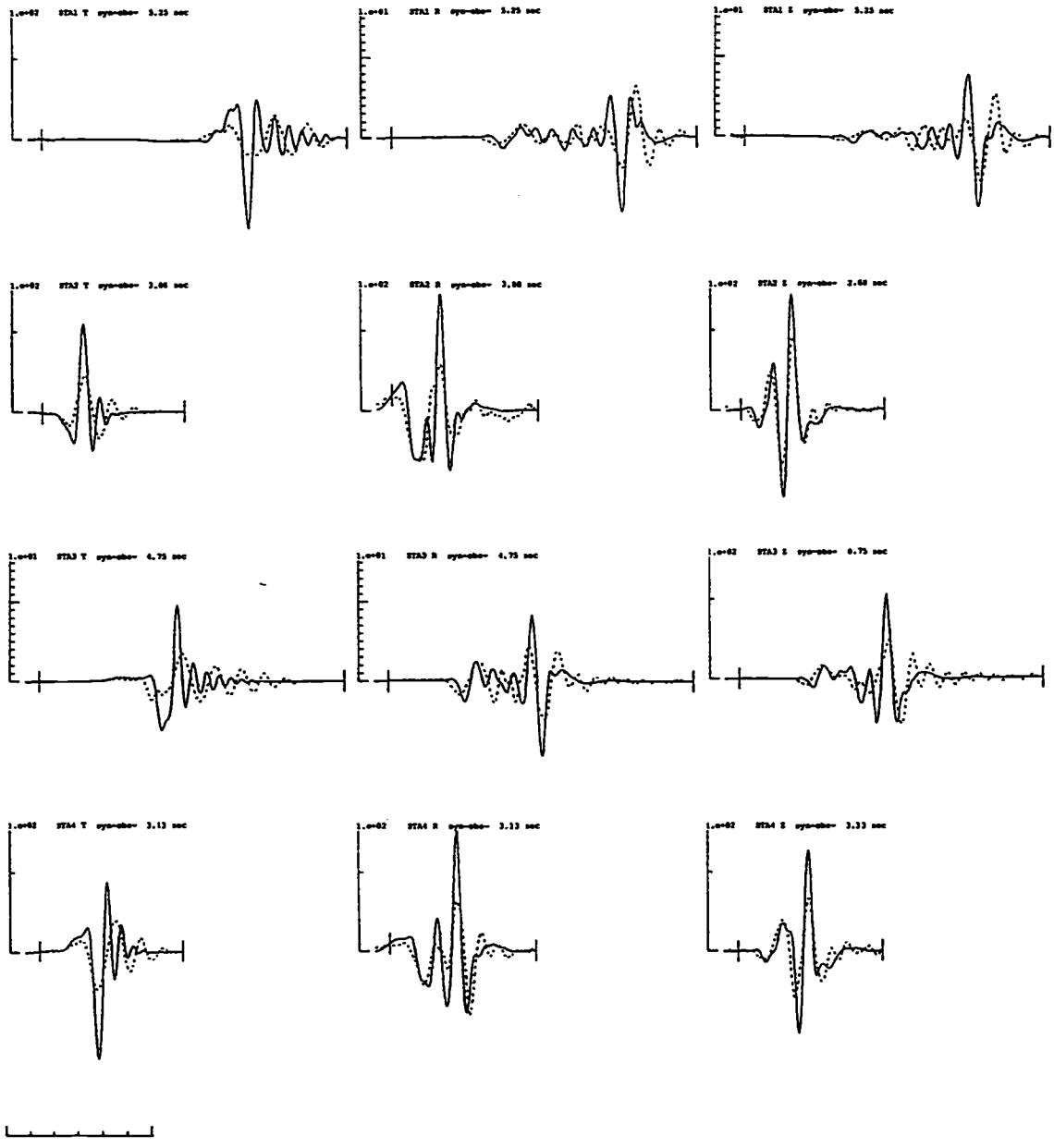

1 minute

Figure 3.3a Sensitivity of the inversion to crustal structure-case II: the thickness of the top layer increases by 3 km. The figure is shown in the same format as figure 3.2a.

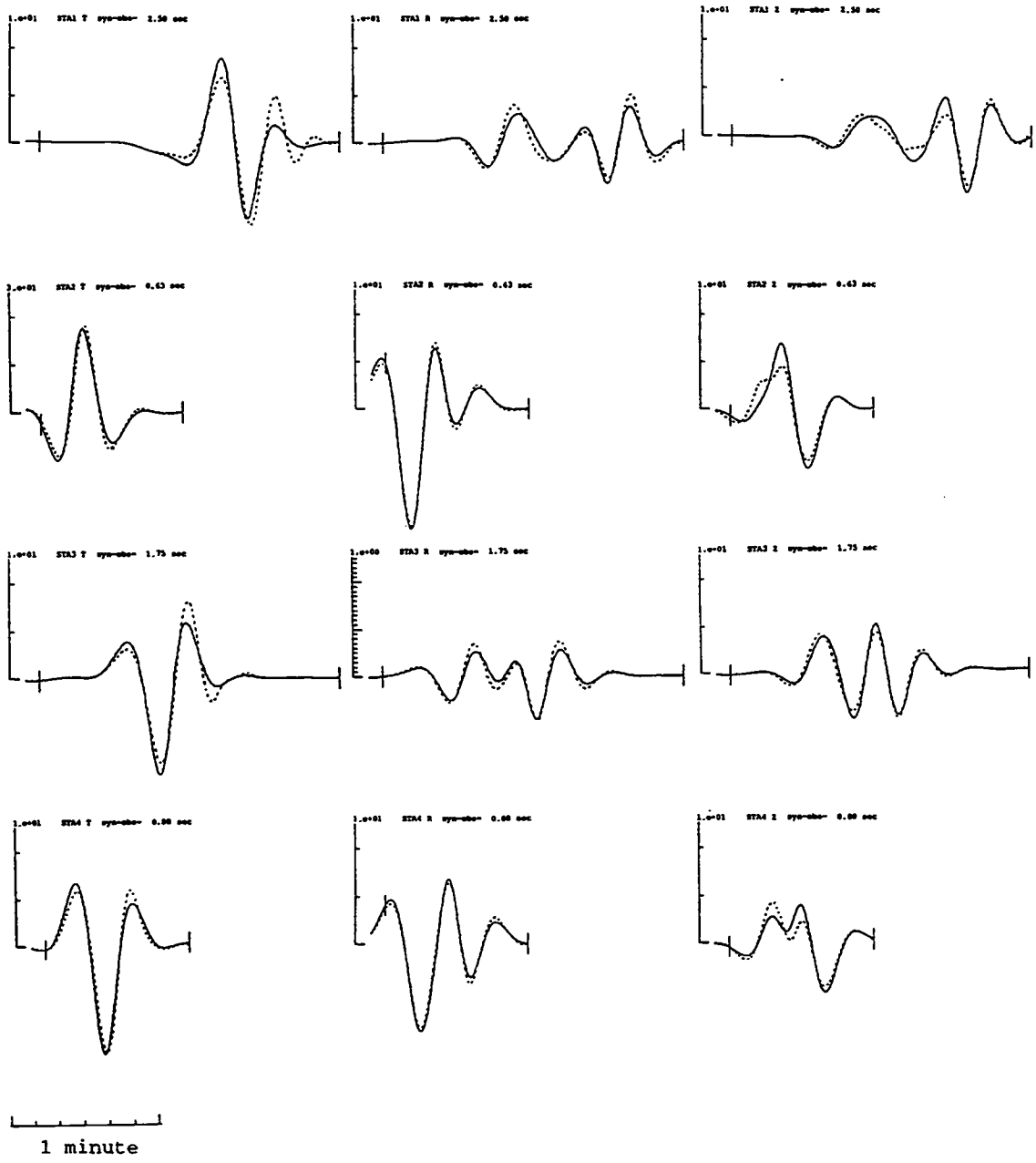

Figure 3.3b Same as figure 3.3a, except for frequencies lower than 0.05 Hz.

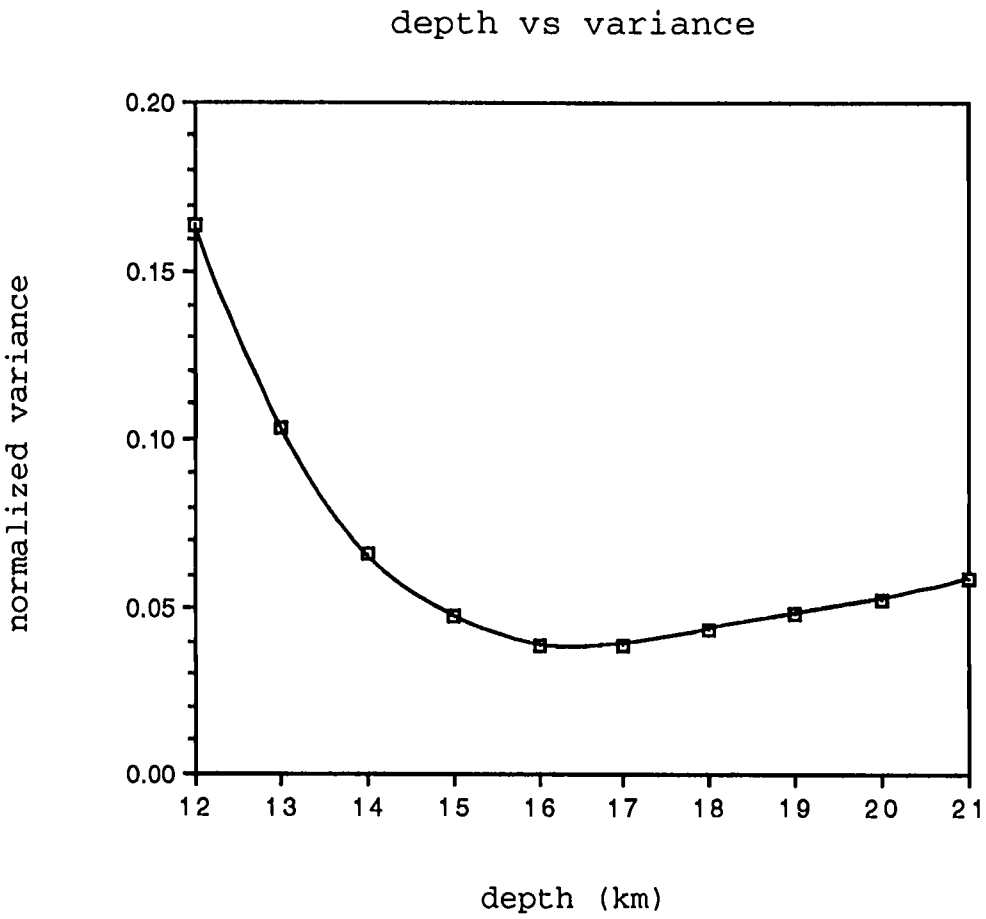

Figure 3.3c The normalized variance is plotted as a function of the source depth showing the effective source depth is greater due to the 3-km thickening of the top layer.

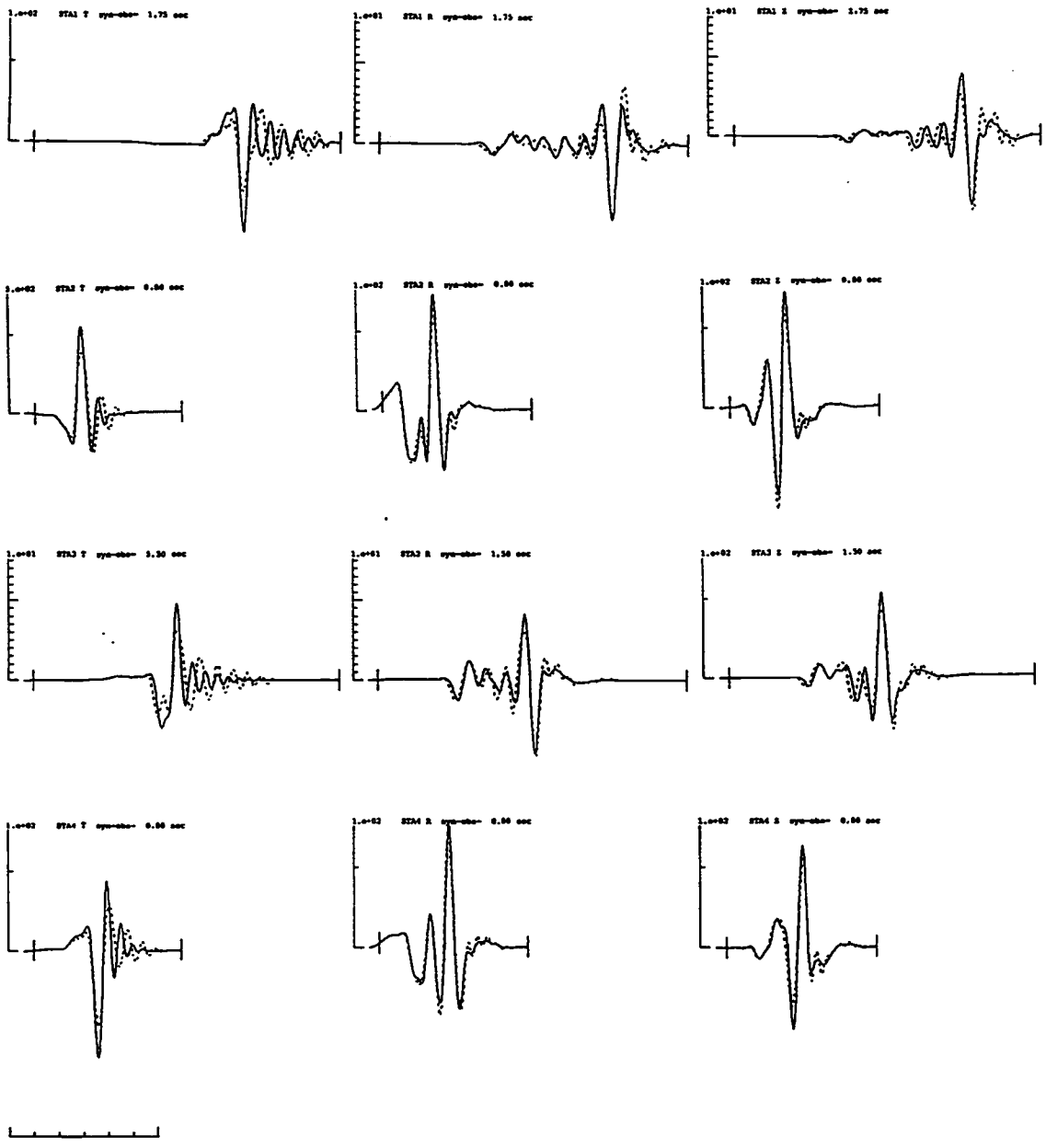

Figure 3.3d Same as figure 3.3a, except for 1 km thickness increase.

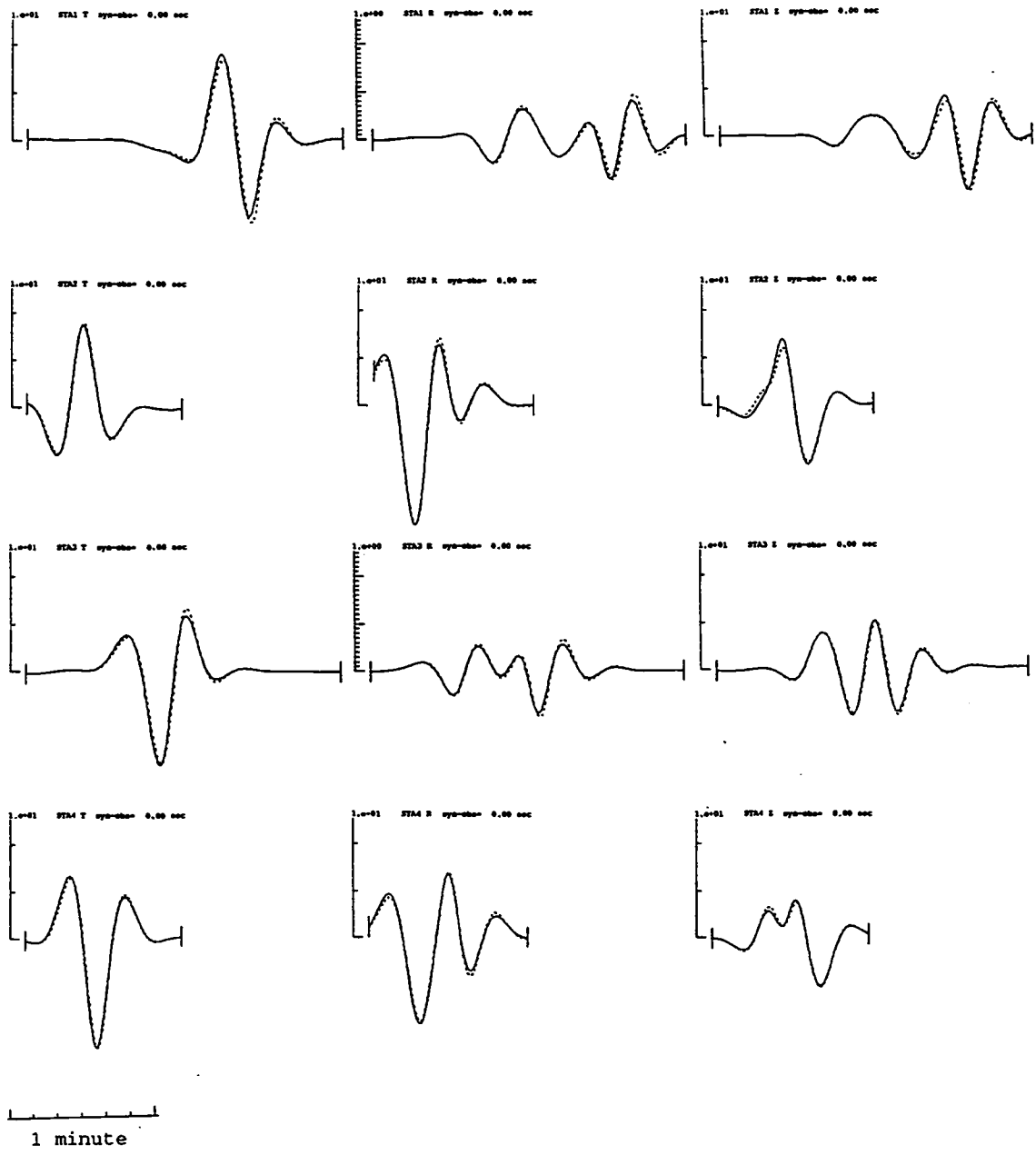

Figure 3.3e Same as figure 3.3d, except for frequencies lower than 0.05 Hz.

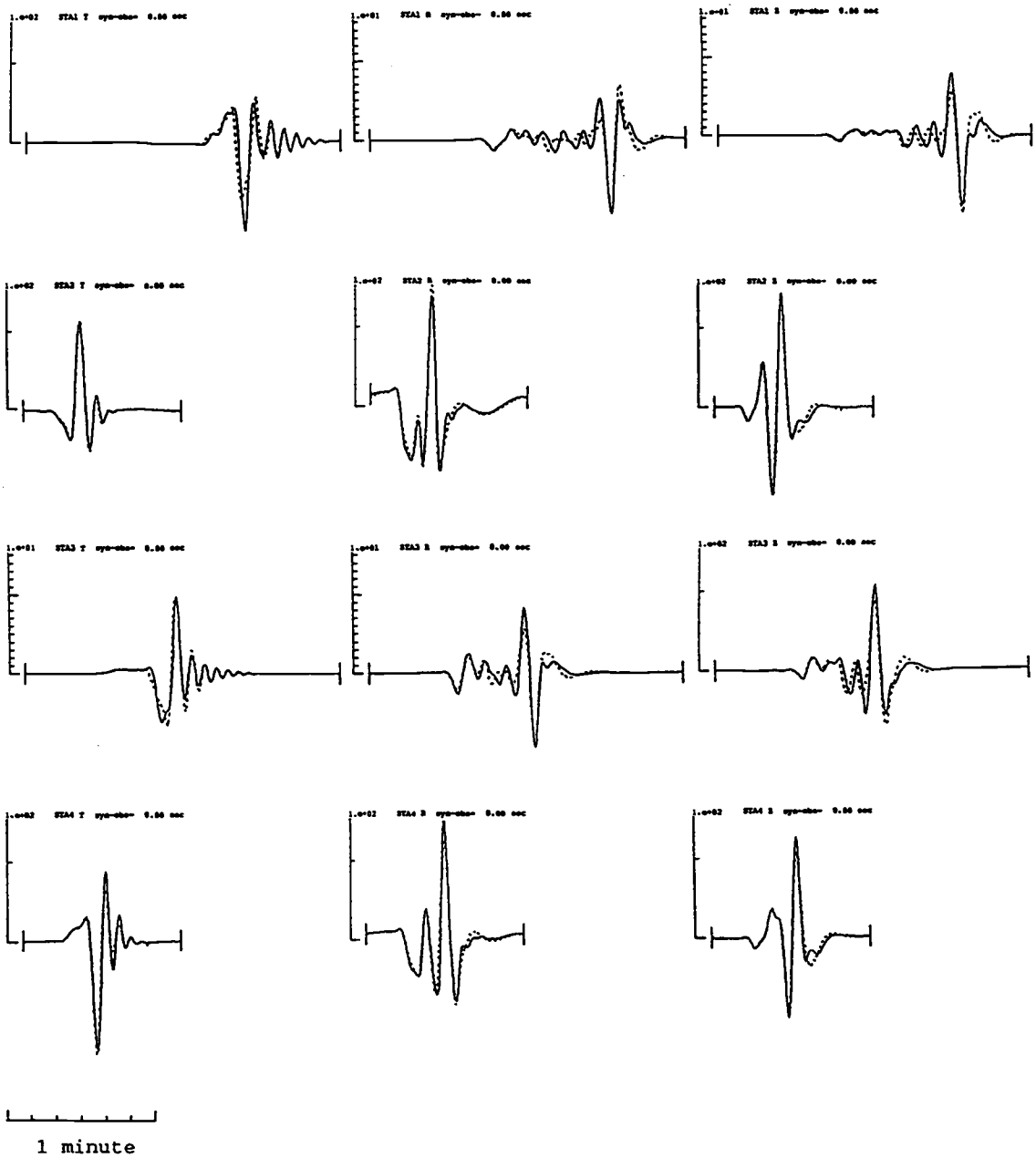

Figure 3.4 Sensitivity of the inversion to crustal structure-case III: the Moho depth shifts up by 5 km. The figure is in the same format as figure 3.2a.

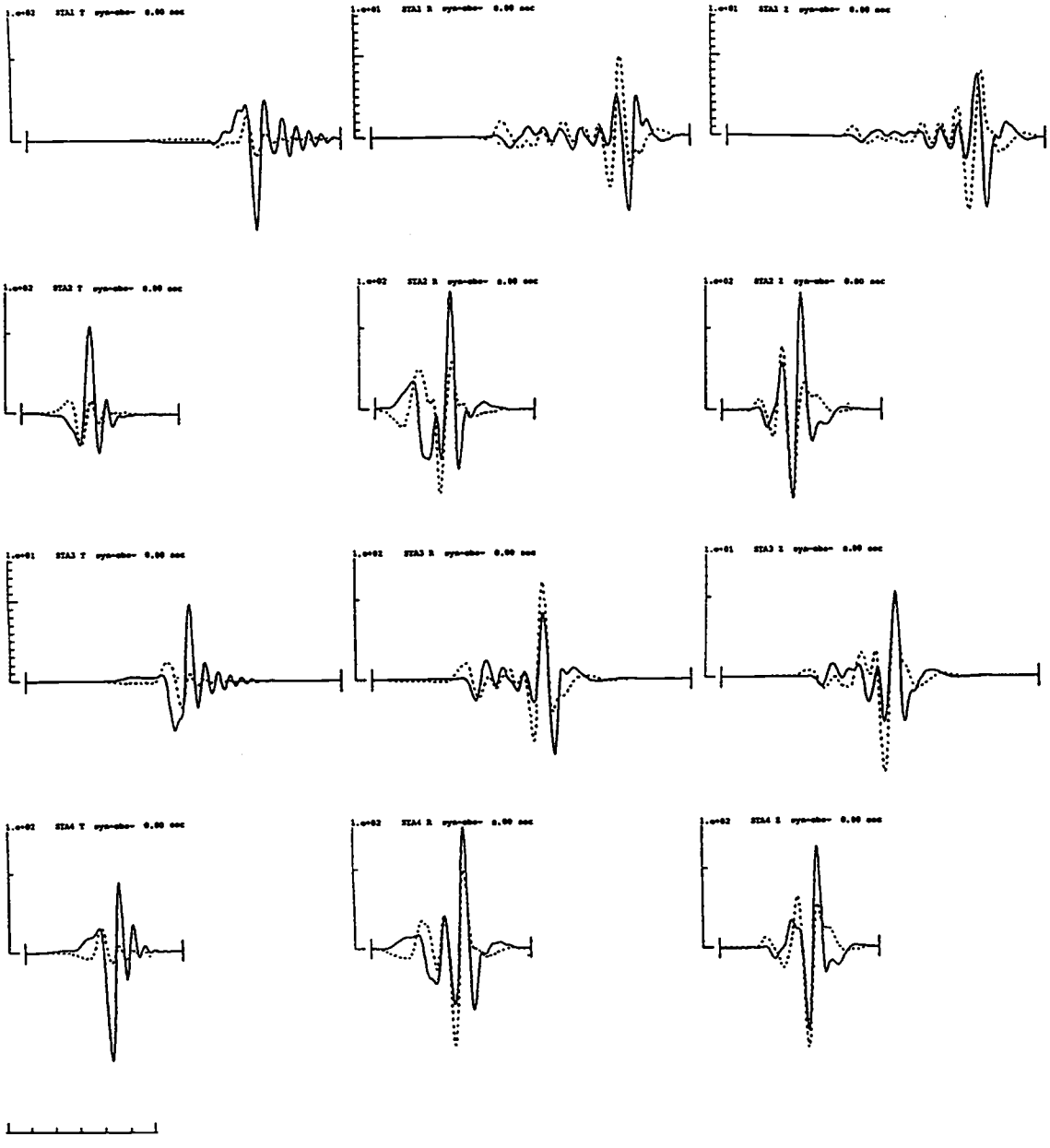

Figure 3.5a Inversion of the seismograms for the event with origin time determined 5 seconds early. Source time function is fixed.

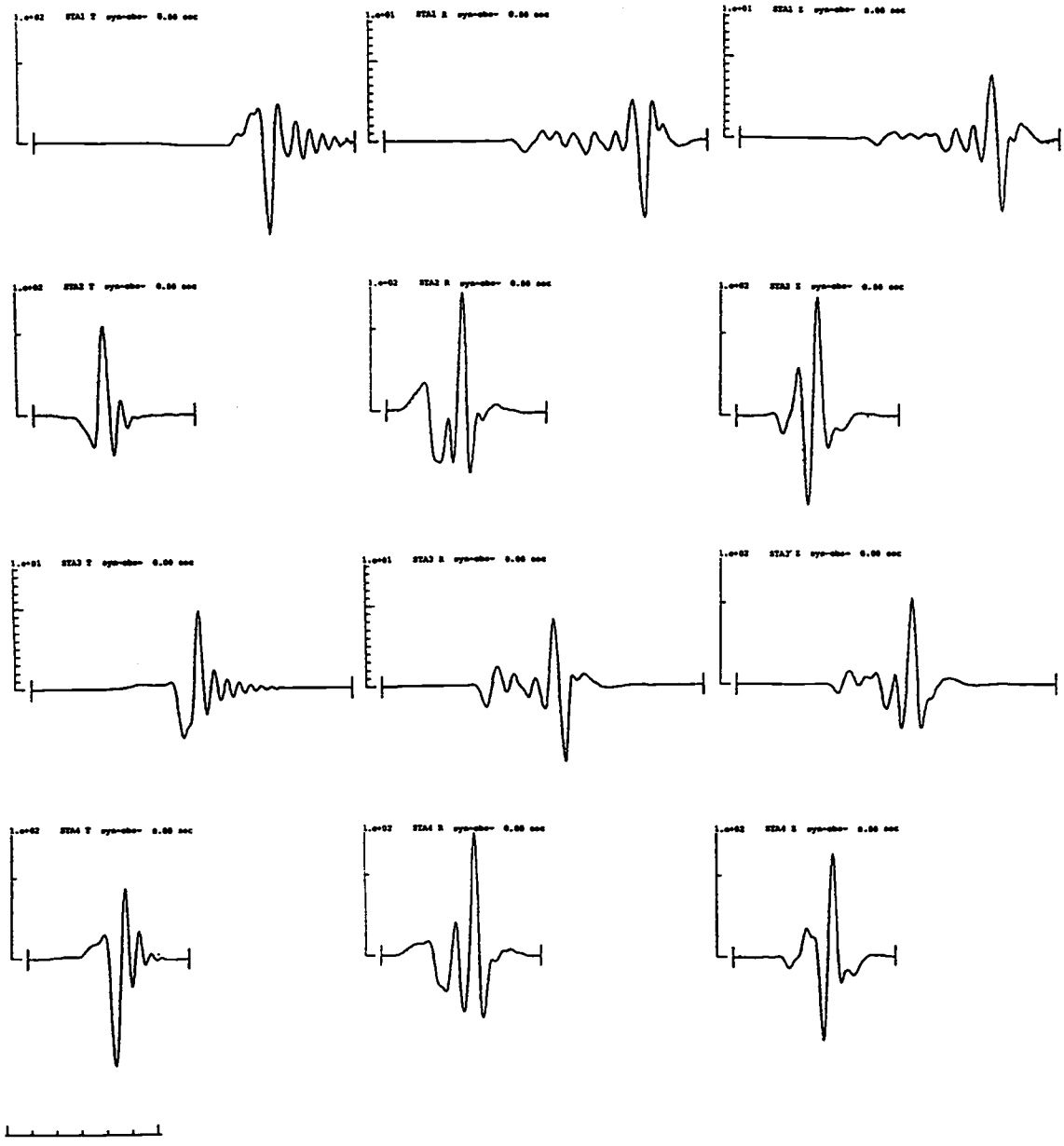

Figure 3.5b Same as figure 3.5a except that now the source time function is allowed to be included as a model parameter. An ideal match is reached.

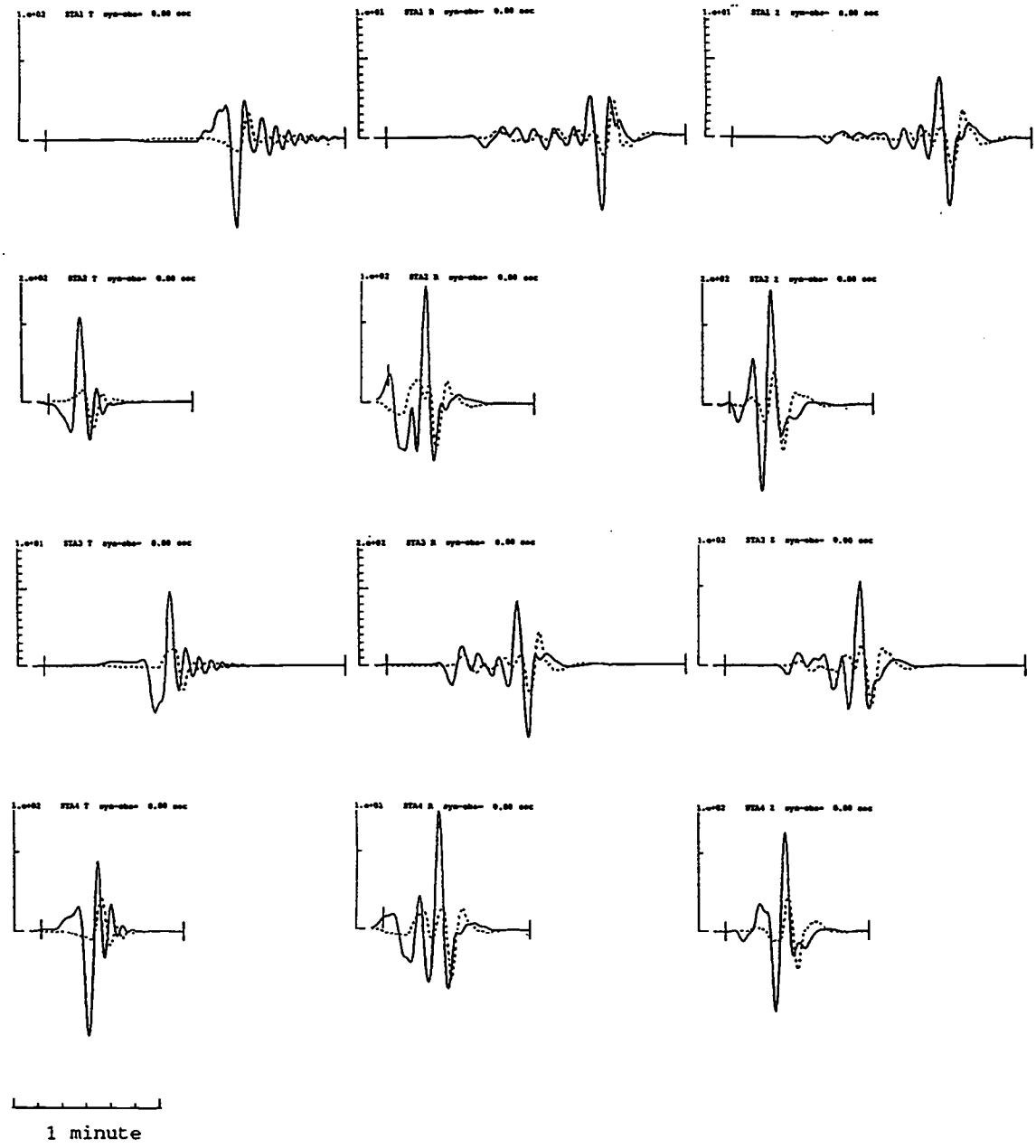

Figure 3.6a Inversion of the seismograms for the event with origin time determined 5 seconds late. Figure shown in the same format as figure 3.2a. No realignment is allowed.

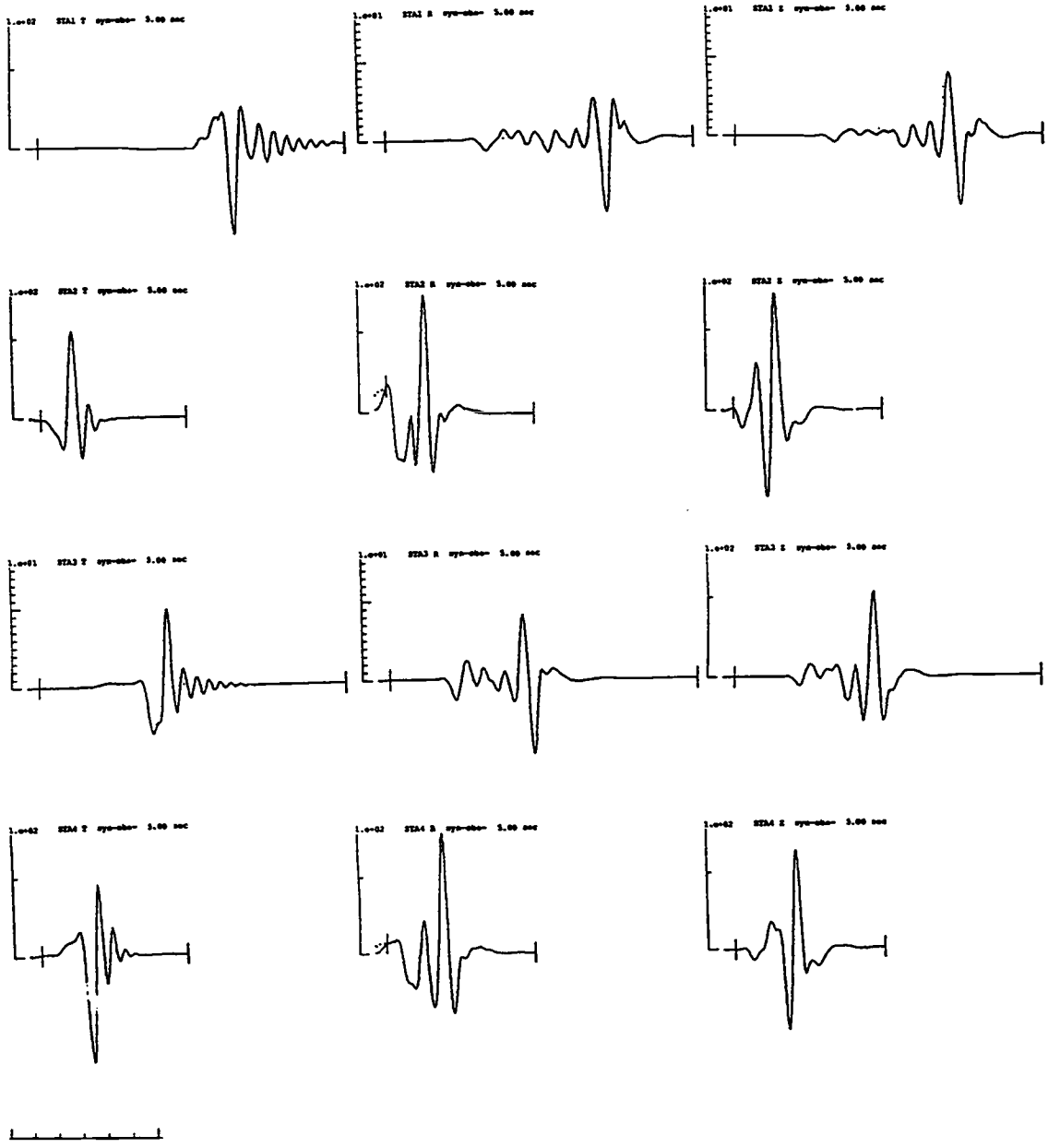

Figure 3.6b Same as figure 3.6a, except that realignment is now allowed, and a perfect match is observed after proper realignment.

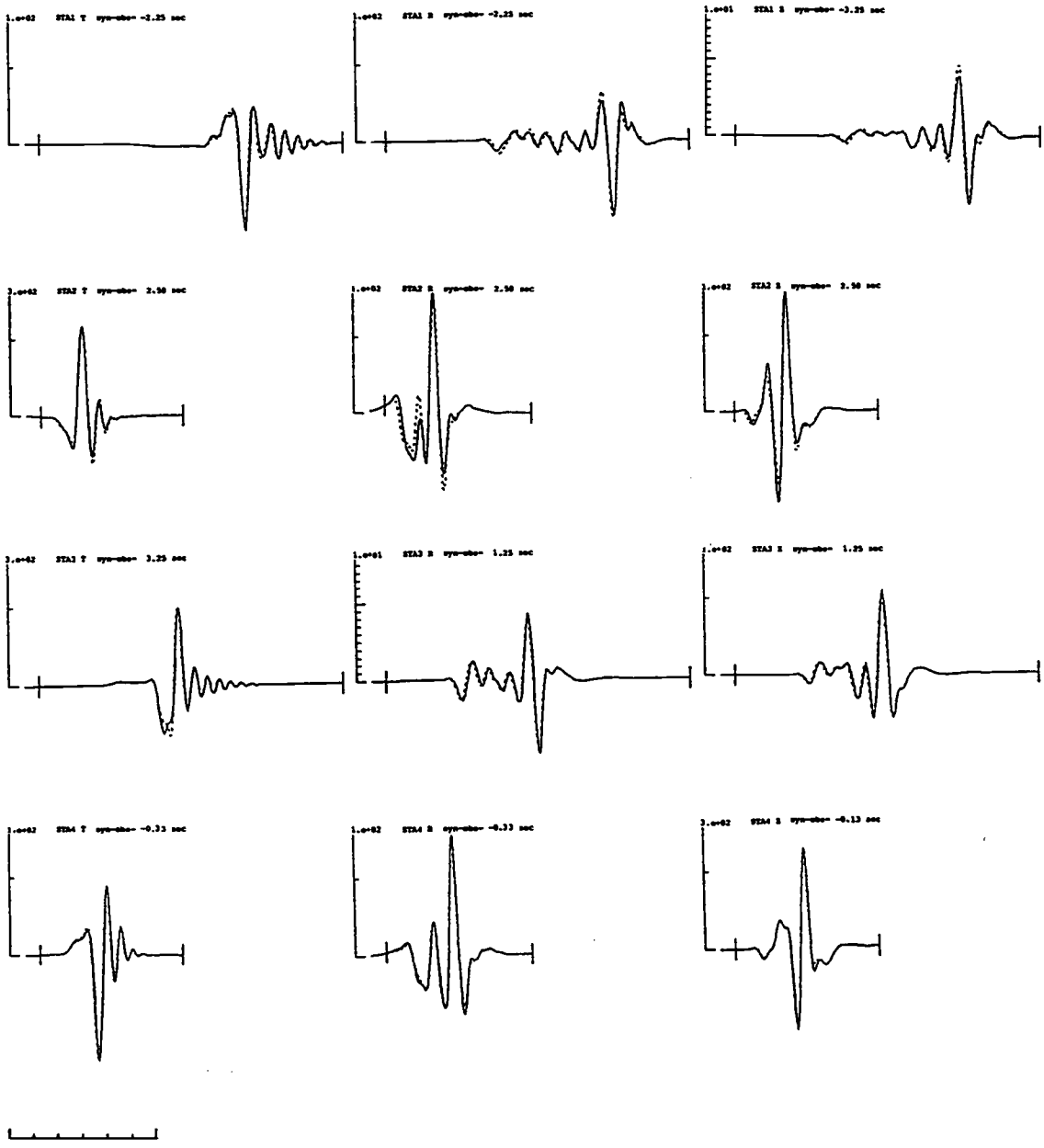

1 minute

Figure 3.7a Inversion of the seismograms for the event located due north of the true epicenter by 10 km. Figure shown in the same format as figure 3.2a. The biggest misfit is observed at the radial component of STA2.

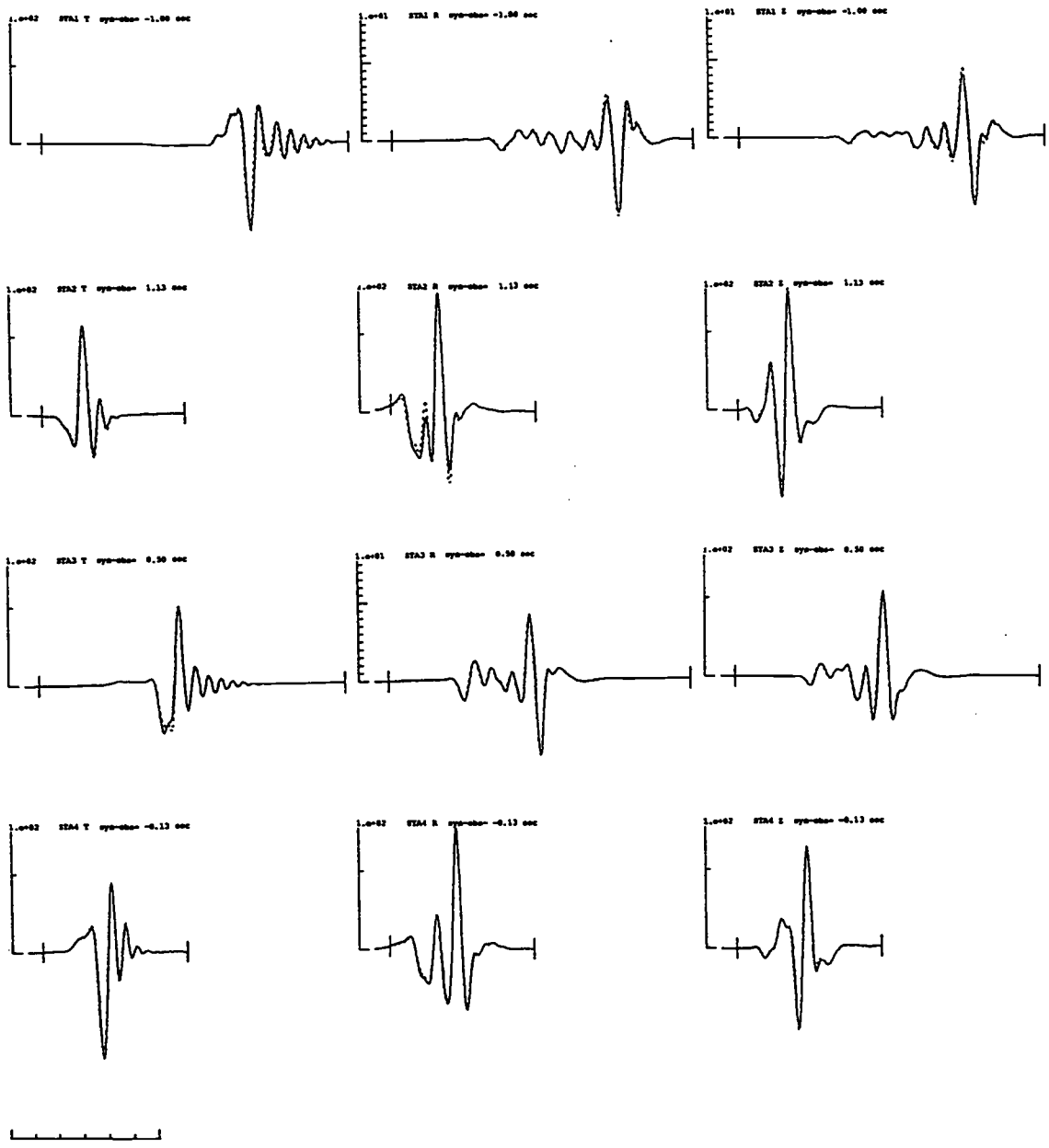

Figure 3.7b Same as figure 3.7a, except that the mislocation is 5 km.

4. Forward Waveform Modeling

Forward waveform modeling is included here to investigate how well the waveforms can be matched at different frequency bands for an earthquake with known parameters. I use the Portland event of July 1991 (m_b=3.5) recorded at the Corvallis station as an example. The epicentral distance to the Corvallis station is about 120 km. This event is large enough to generate sufficient surface waves at frequencies as low as 10 seconds and has been studied previously by Xia and Nabelek (1991). The following is a brief summary of the investigation.

Figure 4.1 shows the broadband data recorded at the Corvallis Station. Figure 4.2a, b, c show waveform match at three frequency bands with a low-frequency cutoff at 0.1, 0.2 and 1.0 Hz respectively. A source mechanism of strike=267^0, dip=70^0, and slip=60^0 from the first motion-polarity readings and a source depth of 15 km were used to compute all the synthetics (the University of Washington and the U.S. Geological Survey information exchange). Of four simple crustal models used for waveform modeling (figure 4.2d), Model D fits the data best. The data are matched very well for frequencies lower than 0.2 Hz. Model D consists of one sediment layer and two crystalline crustal layers overlying the mantle. At frequencies lower than 0.2 Hz, the contribution to the surface-wave energy mainly comes from the upper crust; the Moho is introduced to explaine some wide-angle reflections observed at high frequencies and is not required for modeling lower frequency waveforms. The match at higher frequencies, however, is not adequate to perform an inversion. For this event, 0.2 Hz seems to be the high-frequency limit for an inversion.

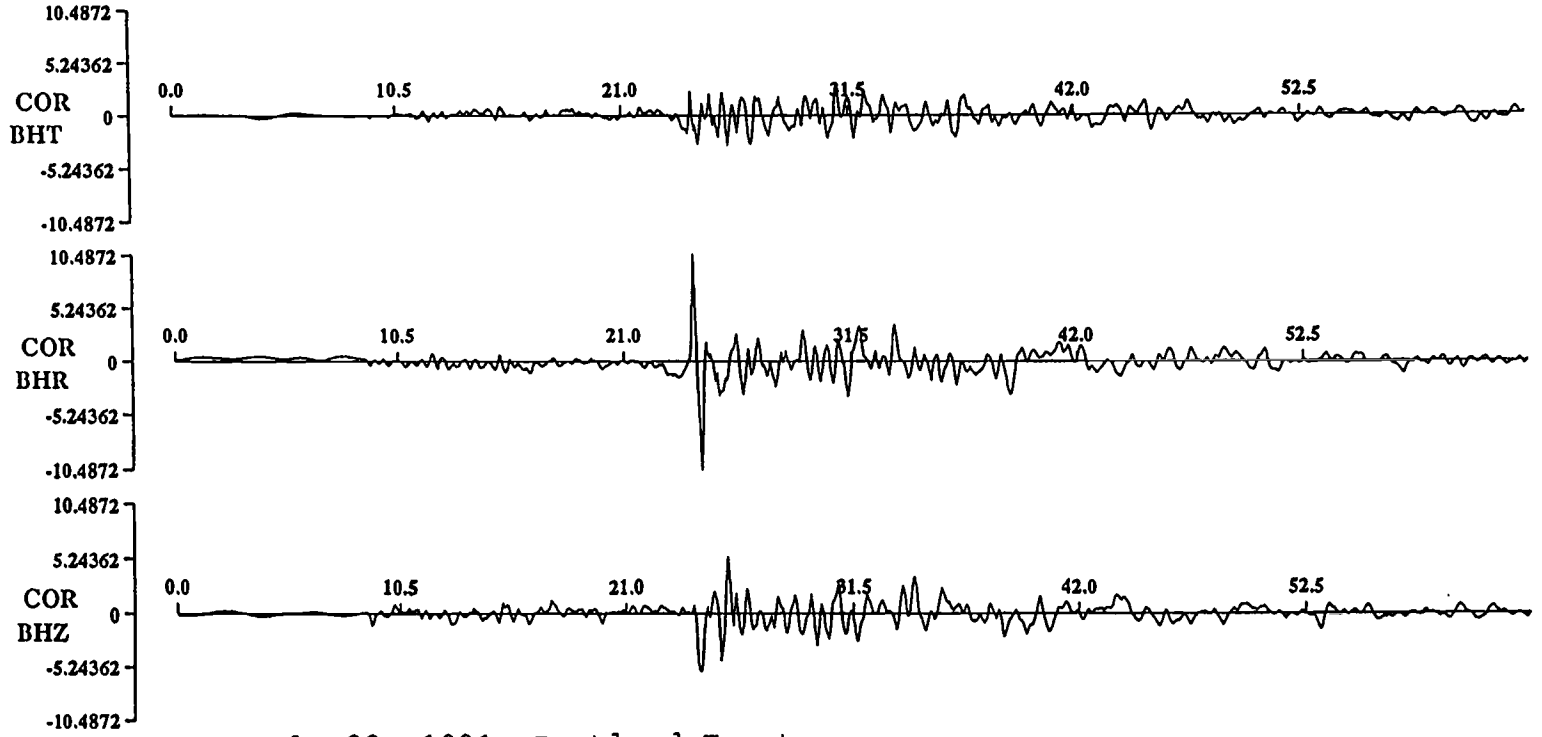

July 22, 1991, Portland Event
Origin Time: 1991/07/22 09:04:38.56
Epicenter: 45.638^0 N, 122.878^0 W
Source Depth: 19.8 km
m_b: 3.5
Source mechanism: strike 267^0; dip 70^0; slip 60^0
Epicentral distance (Corvallis Station): 122.1 km
Back Azimuth (Corvallis Station): 196.1^0

Figure 4.1 The seismograms recorded at at the Corvallis Station for the 1991 Portland event.

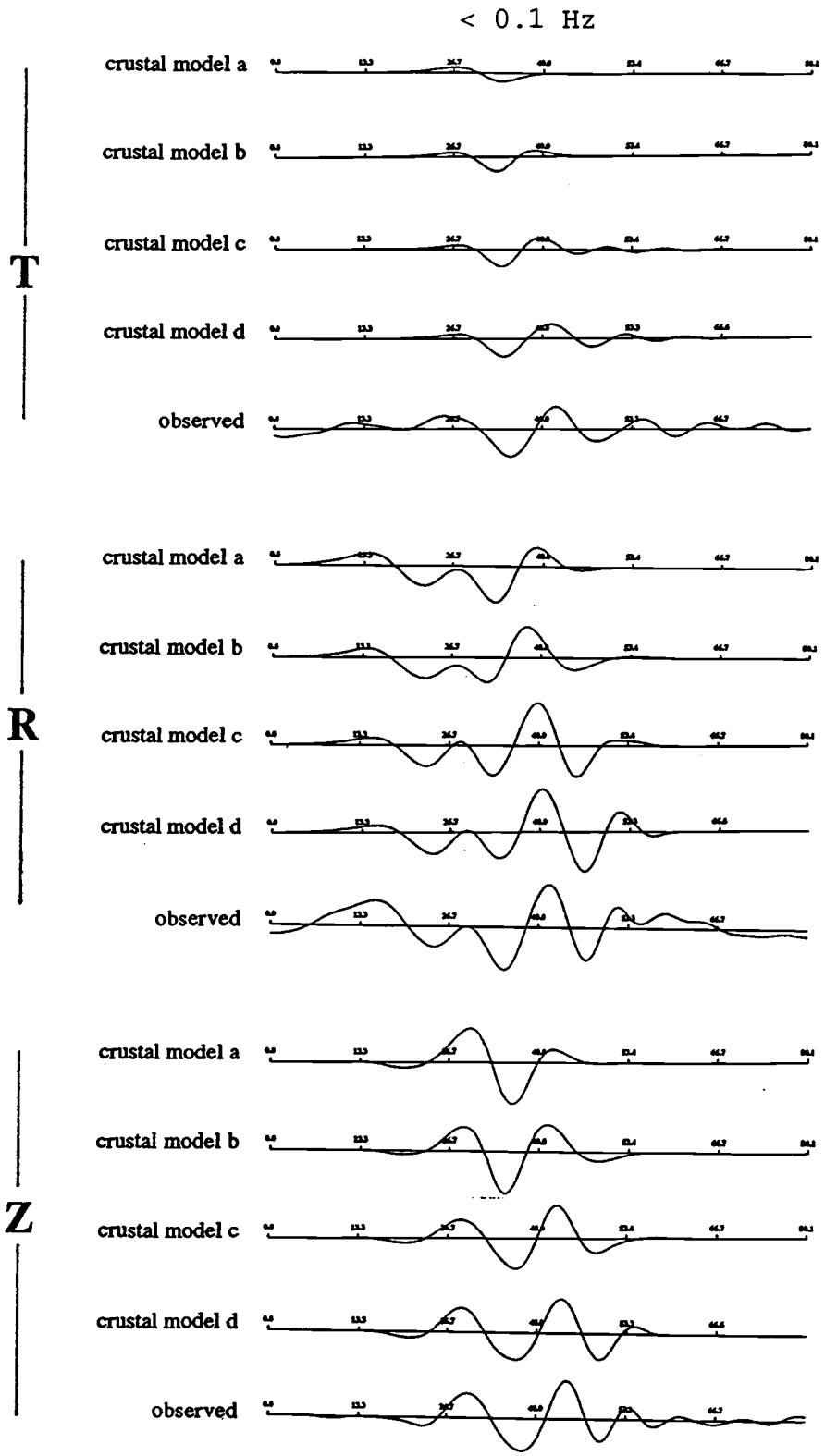

Figure 4.2a Waveform modeling at frequencies lower than 0.1 Hz. The synthetic seismograms are for four crustal models shown in figure 4.2d. Three components: transverse (top group), radial (middle group), and vertical (bottom group), are shown.

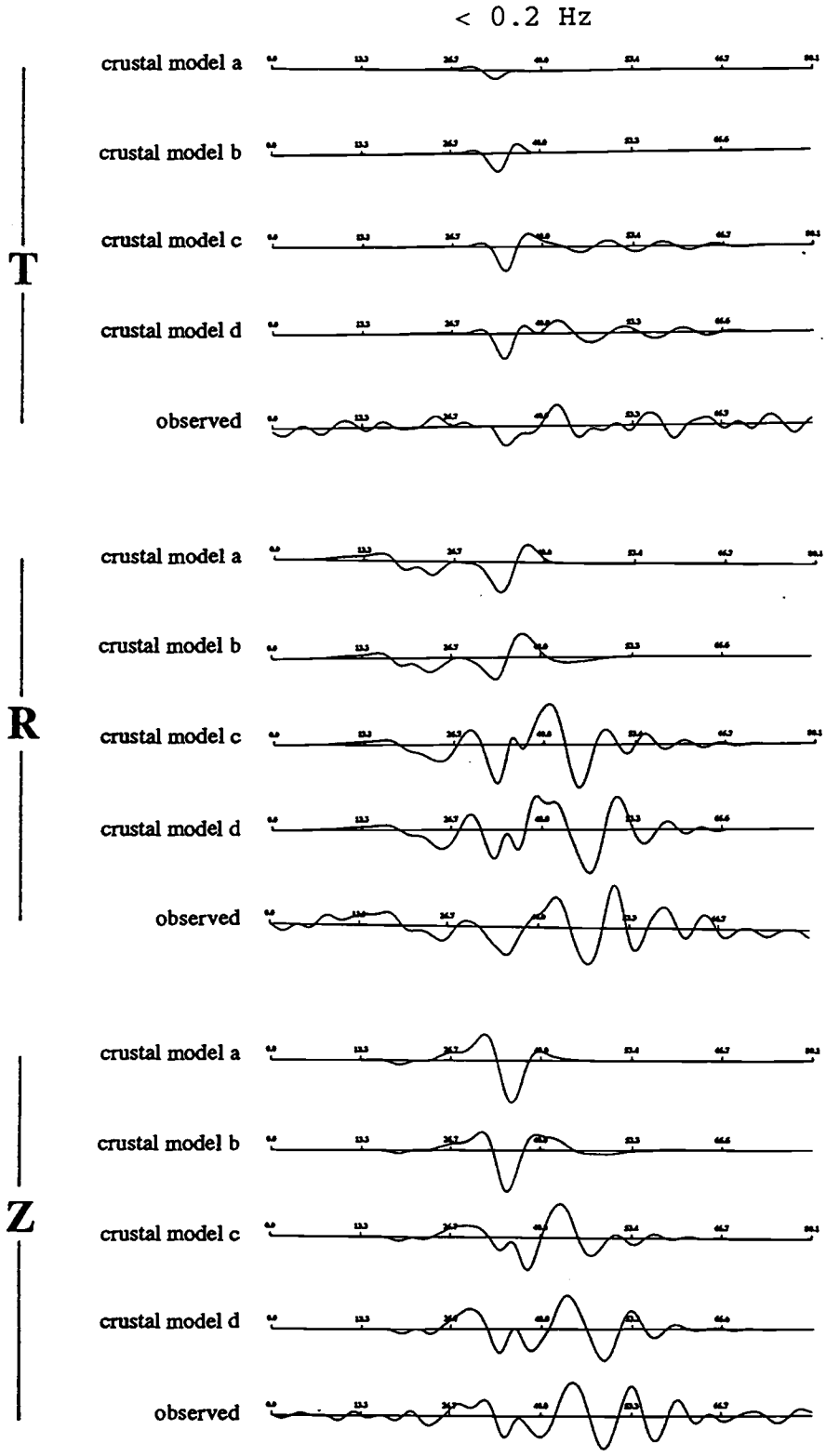

Figure 4.2b Same as figure 4.2a, except for frequencies lower than 0.2 Hz.

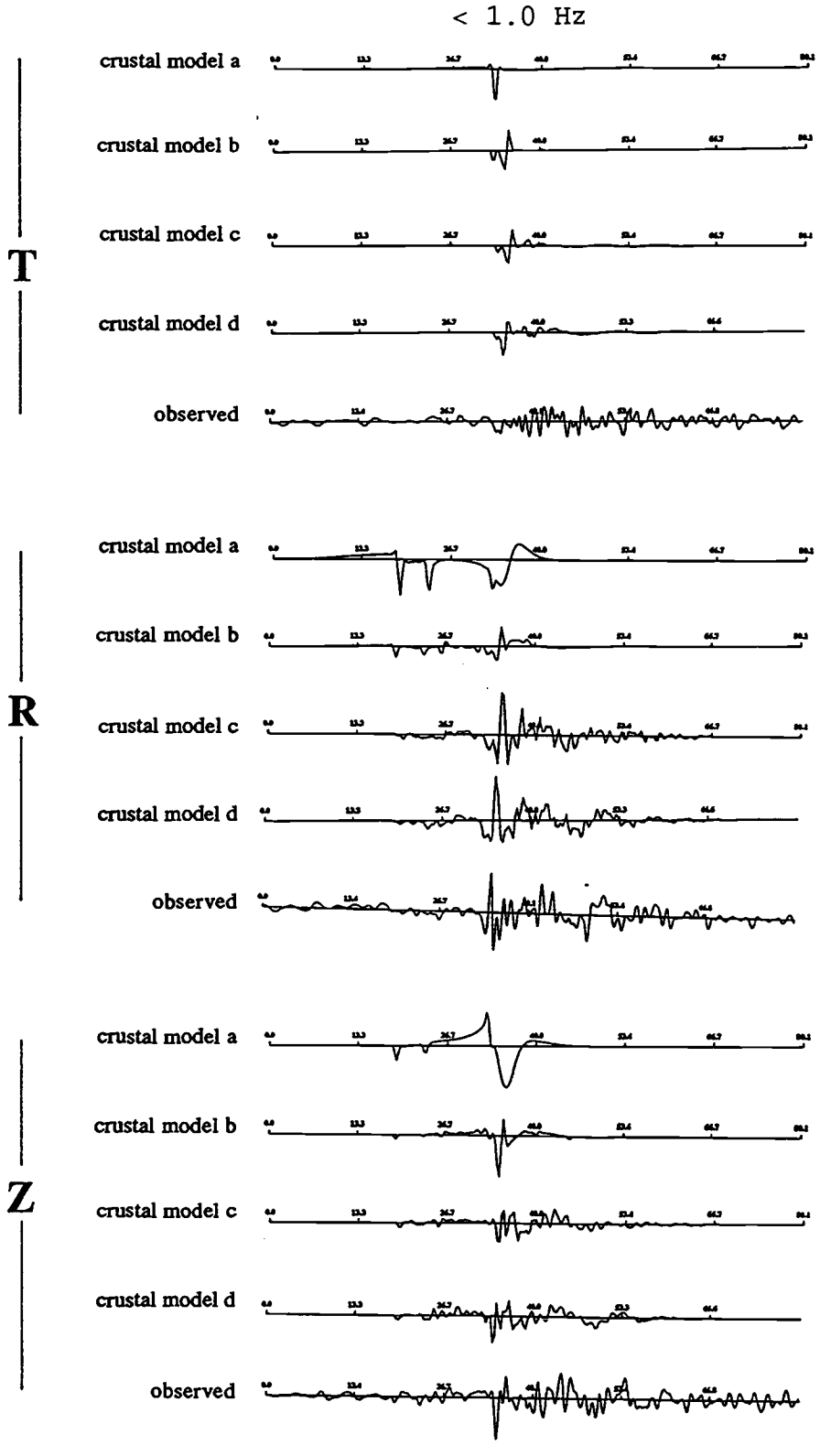

Figure 4.2c Same as figure 4.2a, except for frequencies lower than 1.0 Hz.

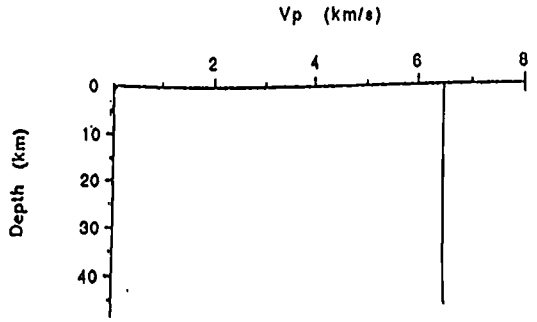

Crustal Model a

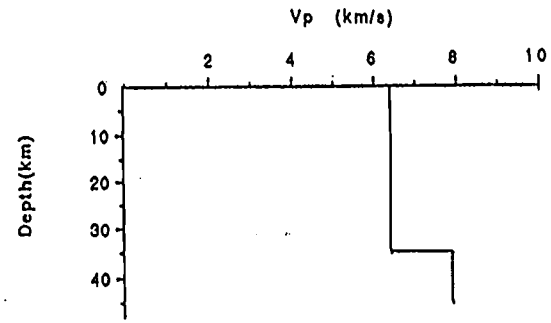

Crustal Model b

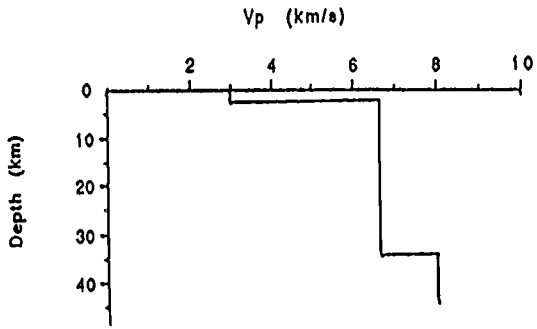

Crustal Model c

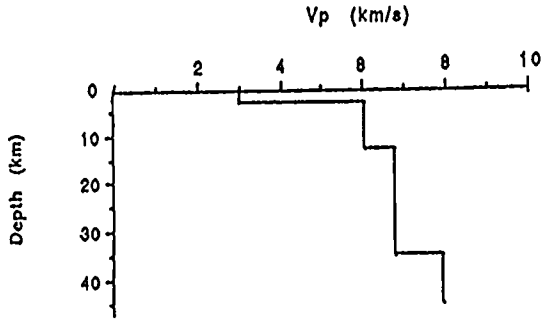

Crustal Model d

Figure 4.2d Crustal models used for generating the synthetics shown in figure 4.2a, b, and c.

5. Inversion for the Scotts Mills, Oregon, Earthquake

In the early morning of March 25, 1993, a strong earthquake (m_b=5.6) occurred near Scotts Mills, southeast of Woodburn, Oregon. The tremor was felt by more than half of the state's population. The quake cracked the marble wall of the state capitol's rotunda, shifted the base of the "Pioneer Statue" on the capitol by 5 mm to the east, and damaged a bridge on Highway 18 near Dayton. A brick wall collapsed at Molalla Union High School during the earthquake (Oregonian, March 26, 1993). The total damage estimate is about $28.4 million according to the assessments by the Oregon Emergency Management Division and the Federal Emergency Management Agency (FEMA) (Madin et al., 1993). This event was the third largest earthquake in the state's history and aroused a tremendous public earthquake awareness. A total of 25 seismometers were set up by the U.S. Geological Survey, Oregon State University, and the University of Oregon within 1 day after the main shock, and 76 aftershocks ranging from 0.9 to 3.2 (m_b) were recorded in the next 25 days (Quarterly Network Report 93-A on Seismicity of Washington and Northern Oregon).

5.1 Local Geology

The most striking geologic structure of the Woodburn area is the Mount Angel Fault, a NNW-trending right-lateral strike-slip fault extending between Woodburn and the Waldo Hills across the northern Willamette Valley (figure 5.1). The fault was identified from seismic-reflection profiles and water-well data, and it displaces the middle Miocene Columbia River Basalt and overlying alluvial deposits (Werner et al., 1992). It has been suggested that the Mt. Angel Fault may be

part of a NW-trending lineament including the Gales Creek Fault, and that the Gales Creek-Mt. Angel Lineament, together with the Portland Hills-Clackmas River lineament, may be a direct consequence of right-lateral motion imposed by oblique subduction. The earthquake swarm (6 events) of August 1990 that occurred on the northwest end of the Mt. Angel Fault had suggested that the Mt. Angel Fault is active.

5.2 Data Processing

Regional data from the Corvallis Station (OSU/IRIS) and Longmire Station (GDSN/IRIS) are available for the 1993 event. The origin time and the epicenter are well determined by the Washington Regional Seismic Network (WRSN). Table 3 lists the event and station information. All the data are first high-pass filtered with a cutoff frequency at 0.01 Hz, and converted to broadband-displacement records. Different time windows for inversion are assigned to each station according to their epicentral distance (64 seconds for COR, and 128 for LON). The data are down-sampled to 4 and 2 samples per second for COR and LON, respectively. Two different sampling rates are chosen to give an equal number of points to each station.

I adapted the crustal structure of Trehu et al. (1992) for the COR path from the recent wide-angle reflection and refraction experiment conducted in western Oregon (figure 5.2). The upper crustal structure is constrained very well; the 6 km thick lower velocity zone (LVZ) is constrained from a receiver-function study (Li et al., 1992). The only change made for the LON path is that it has only a 1 km thick sediment layer. A Possion ratio of 0.27 is used to match the P and S direct arrival times for both paths. The attenuation is also assumed, with a Q factor of 225 for the compressional

waves and 100 for the shear waves. These Q values are not well constrained, but the effect at low frequencies is small.

5.3 Inversion Procedures

Because this is a crustal event, I did not consider the volume change of the source process. Therefore, a firm deviatoric constraint on moment-tensor elements is applied throughout the inversion. Ten triangular source time functions, each with the same 1-second half duration are included as part of the model parameters, to resolve for a possible complicated source process. The damping factor was applied from time to time to low-pass filter the model parameters, and was set each time to be slightly larger than the singular values of those model parameters I wished to filter out. Both the observed and synthetic data are normalized to the epicentral distance of the LON station (surface wave type normalization) to give equal weight to each station. The iteration was stopped when no more improvement to the fits between the observed data and the synthetics was observed. The realignment was performed to maximum the cross correlation, and the iteration restarted over and over again until the minimum residual of the fit was reached.

5.4 Inversion Results

To see in which frequency band the best match can be reached, the inversion is performed first in three different frequency bands, namely, from 0.04 Hz to each of 0.2, 0.1, and 0.05 Hz (figure 5.3a, b, and c). The observed data at LON are quite noisy below 0.04 Hz; therefore, 0.04 Hz was

chosen as the lower frequency limit. For the LON record, the waveforms do not match in the 0.04-0.05 Hz, possibly due to the remaining high noise level in this narrow band. The inversion in the 0.04-0.05 Hz band gives a source mechanism of strike=308^0, dip=40^0, and slip=165^0 with 89% double-couple component. The fit in the 0.04-0.2 Hz band is not bad, except for small amplitude discrepancies for three components of COR, and slight phase shifts of surface waves for LON. The inversion performed in the 0.04-0.2 Hz band yields a source orientation of strike=324^0, dip=72^0, and slip=160^0 with 90% double-couple component. The waveforms are matched best in the 0.04-0.1 Hz band. The inversion in this frequency band gives a source orientation of strike=316^0, dip=51^0, and slip=162^0 with an 85% double-couple component (figure 5.4). The resolved source duration is about 2 seconds and the seismic moment is 2.8×10^{24} dyn cm which corresponds to magnitude 5.6 (M_w). The realignment did not improve the waveform matches, so the time shifts for both stations were zero.

Normalized variance is plotted as a function of source depth (figure 5.5), which gives a well defined minimum between 10 and 15 km.

In figure 5.6, the normalized variance is plotted as a function of the source-orientation deviation from the best-fit model. The best-fit orientation is fairly well constrained by the inversion.

The inversion result yields a right-lateral strike-slip fault-plane solution with the strike of one fault plane parallel to the Mt. Angel Fault, strongly suggesting this event may be related to the Mt. Angel Fault.

Table 3. Event and station parameters for the Scotts Mills earthquake.

Event parameters from the Washington Regional Seismic Network:

Year	Month	Day	Time	Lat(^{0})	Lon(^{0})	m_b	Depth (km)
1993	03	25	13:34:35.44	45.004	-122.607	5.6	20.6

Station parameters:

Station	Δ(km)	Azimuth (^{0})	Instrument Type
COR	74.4	228.7	STS-1
LON	201.4	17.5	S-5007

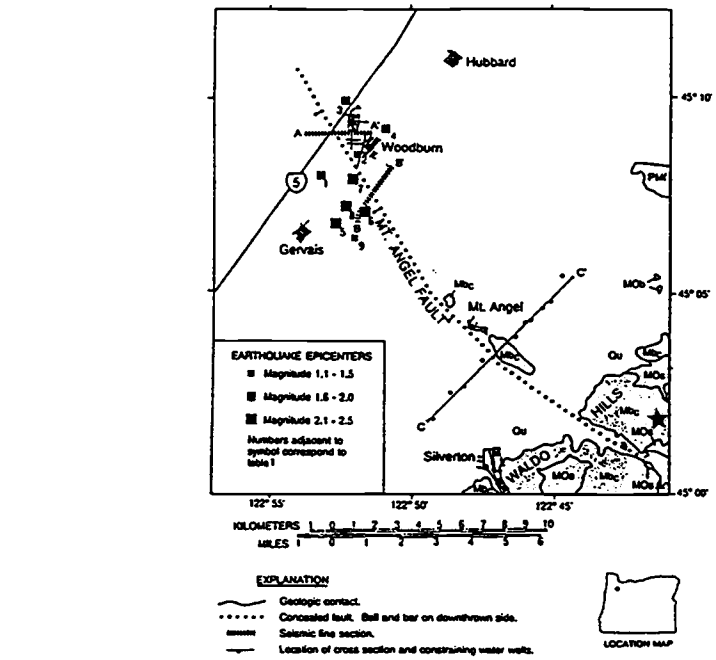

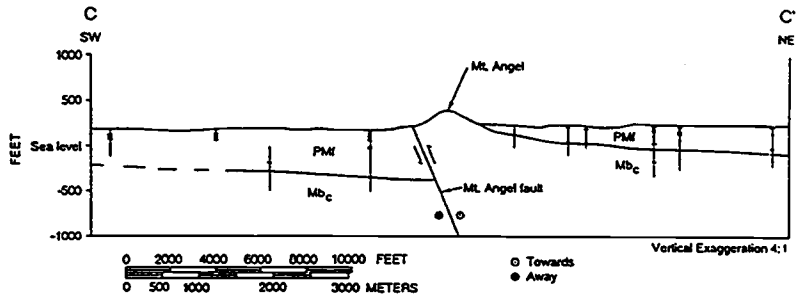

Figure 5.1 Geologic structure of the Woodburn area. The top figure shows the Mt. Angel Fault (dotted line) and a swarm of small earthquakes (solid squares) that occurred on August 1990. The epicenter of the Scotts Mills event in this study is indicated by a star. The bottom figure is the structure cross section C-C' in the top figure (from Werner et al., 1992).

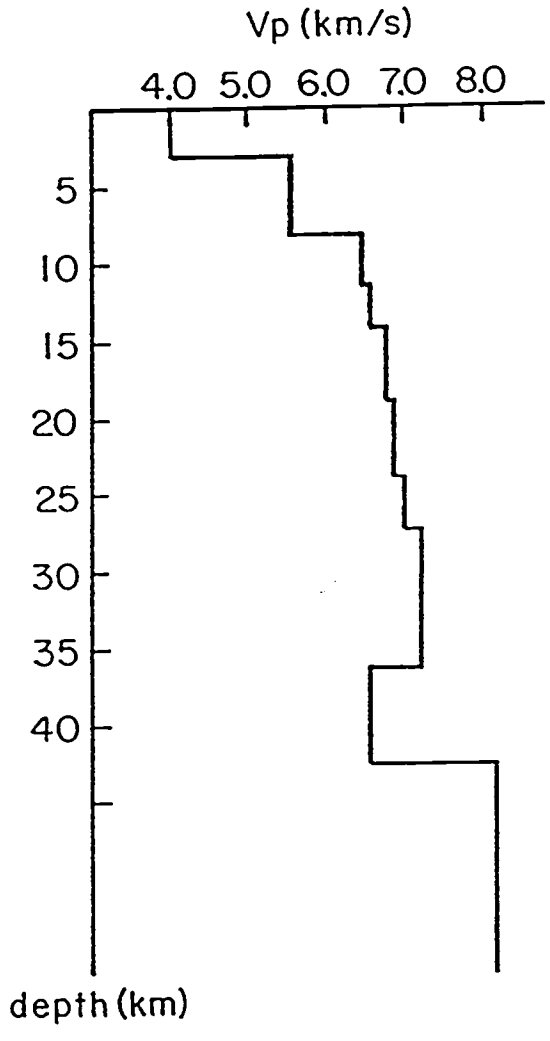

Figure 5.2 Crustal structure of the Willamette Valley from recent reflection and refraction profiles (Trehu et al., 1992) and a receiver-function study (Li et al., 1992).

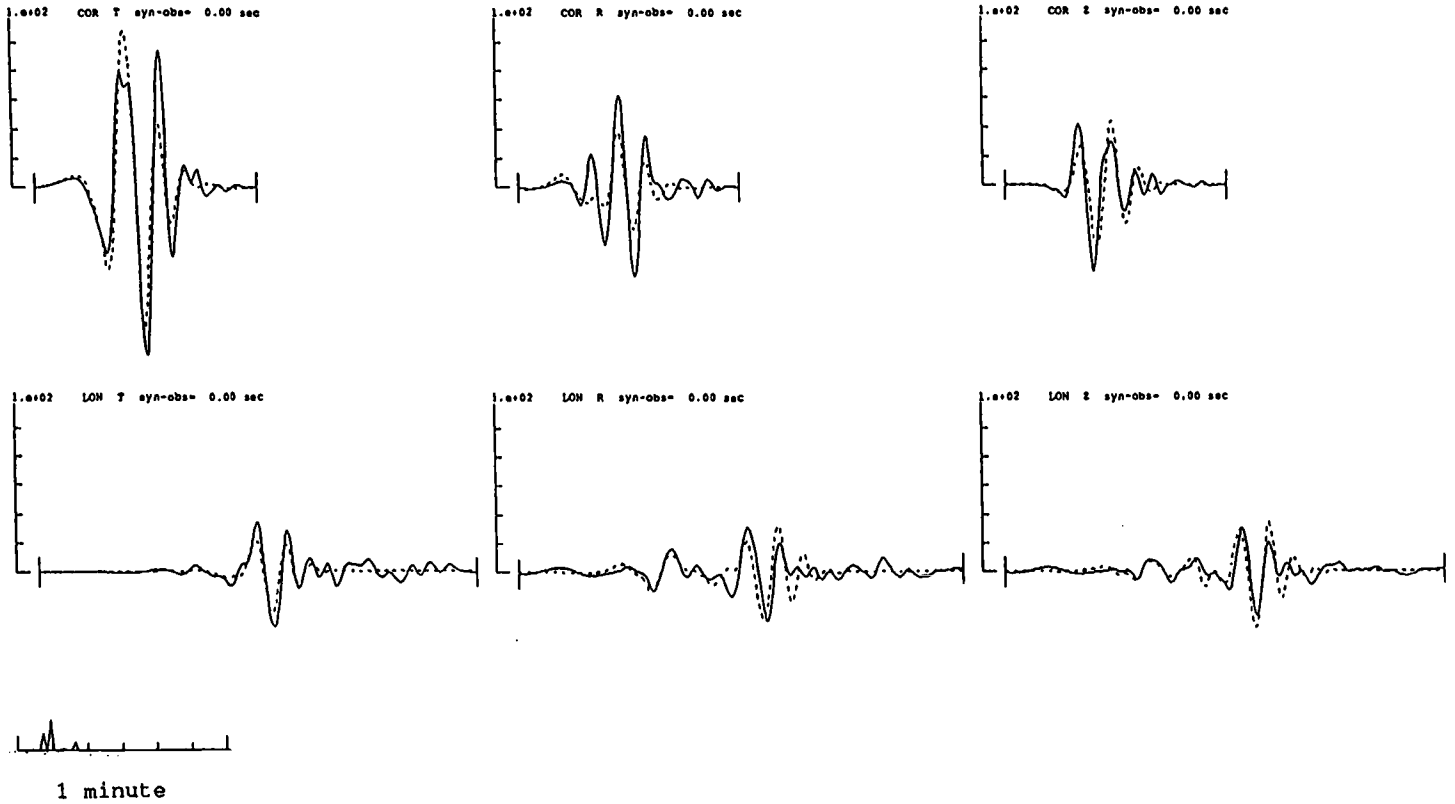

Figure 5.3a Inversion of the seismograms for the Scotts Mills event in 0.04-0.2 Hz. The solid lines are for the observed data and dash lines for the synthetics. Stations COR (top) and LON (bottom) are shown. Traces from left to right are for transverse, radial, and vertical components, respectively. The source time function is shown in the left-bottom corner.

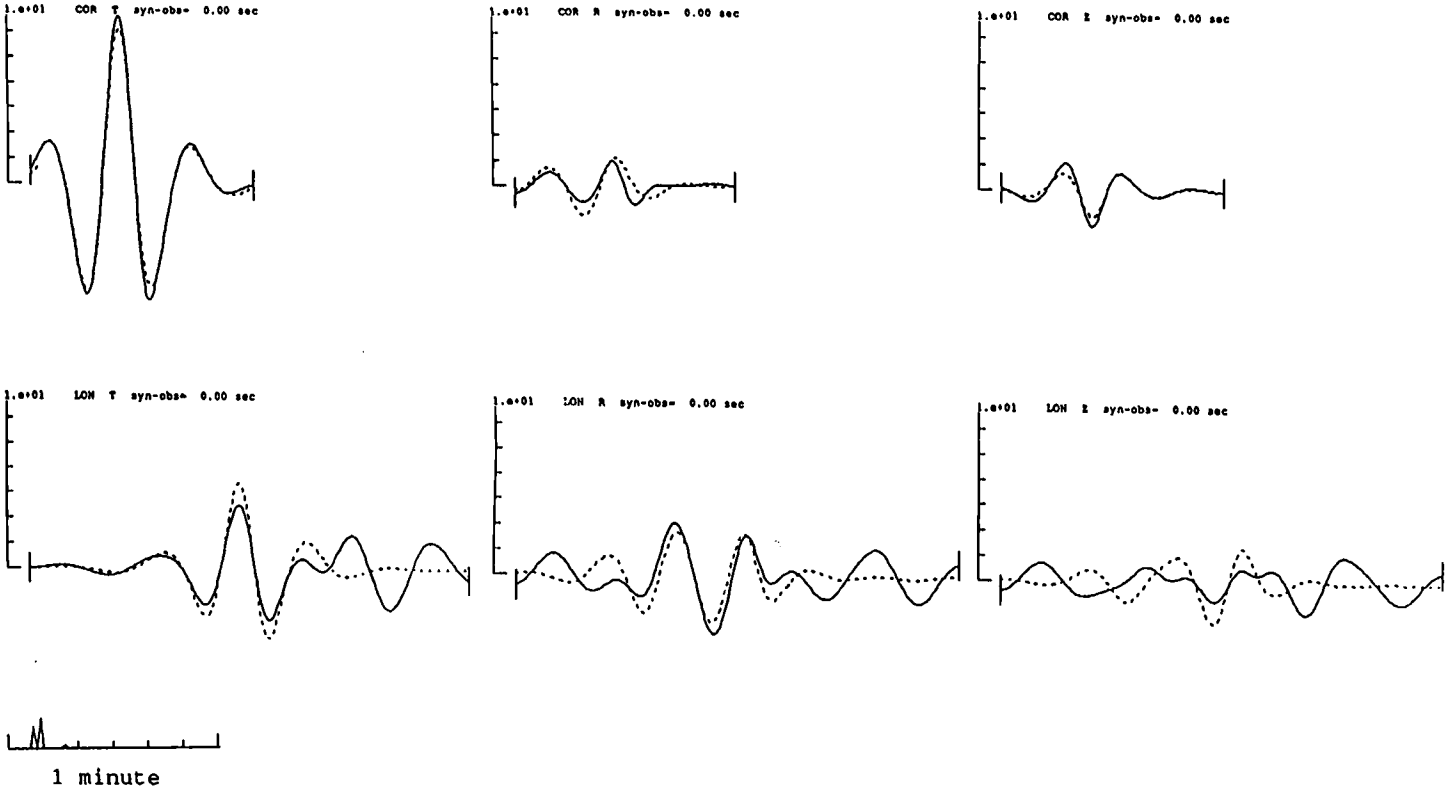

Figure 5.3b Same as figure 5.3a, except for frequencies in 0.04-0.05 Hz.

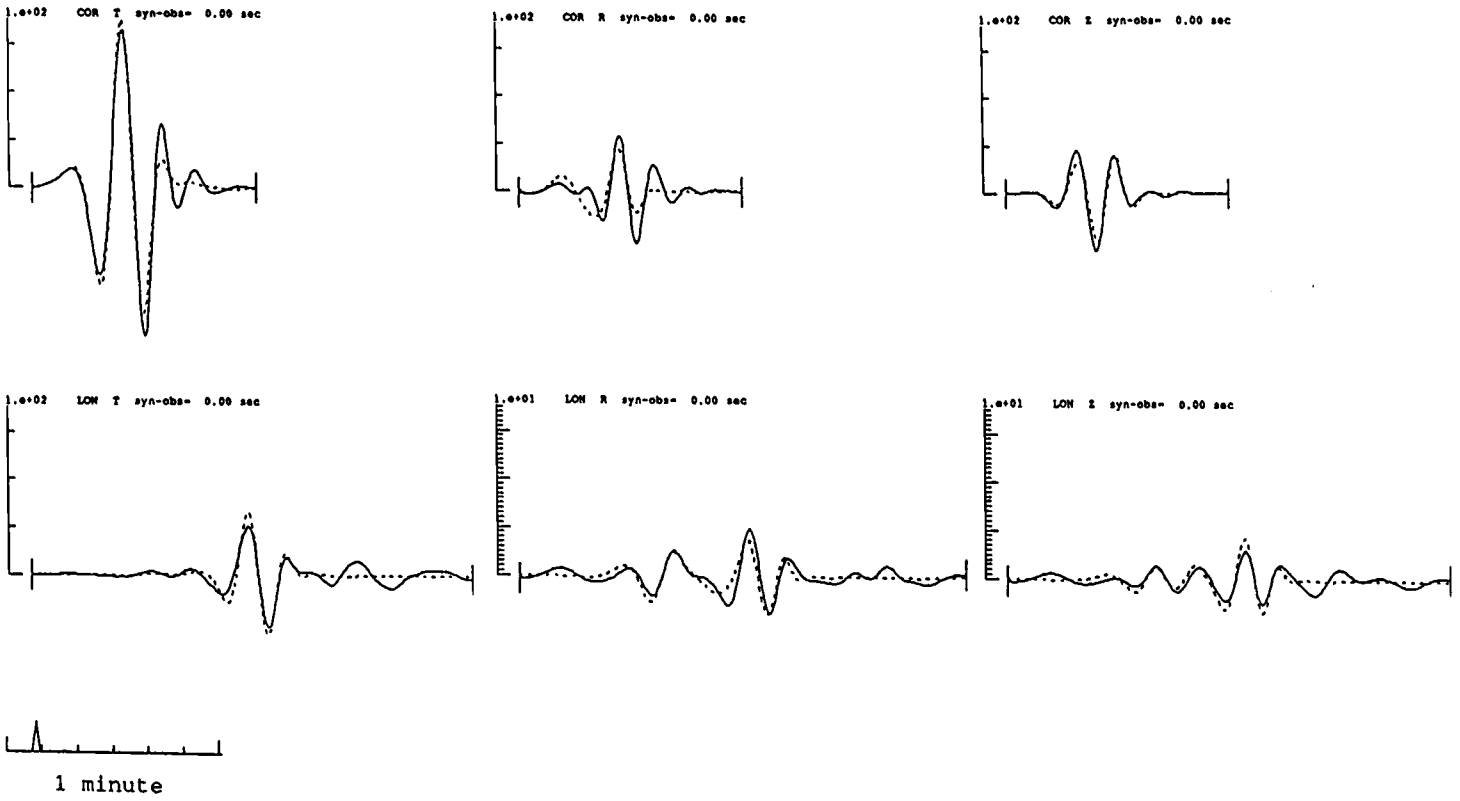

Figure 5.3c Same as figure 5.3a except for frequencies in 0.04-0.1 Hz. This is the preferred frequency band used for the inversion of this event.

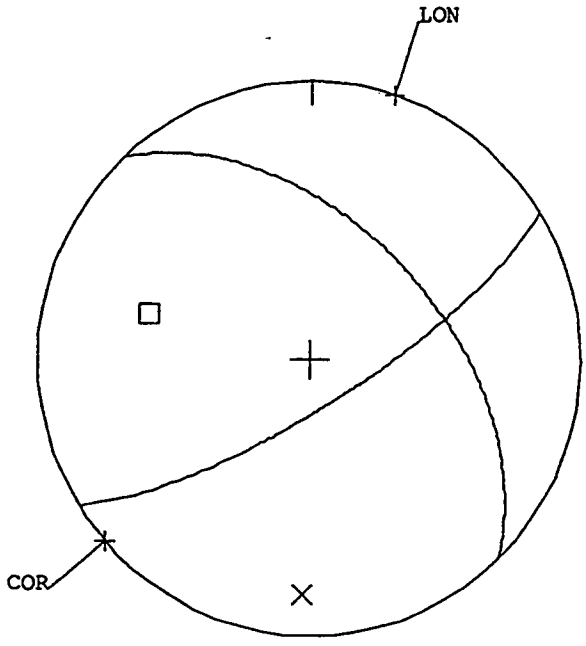

Figure 5.4 Fault-plane solution from inversion of the seismograms for the Scotts Mills event.

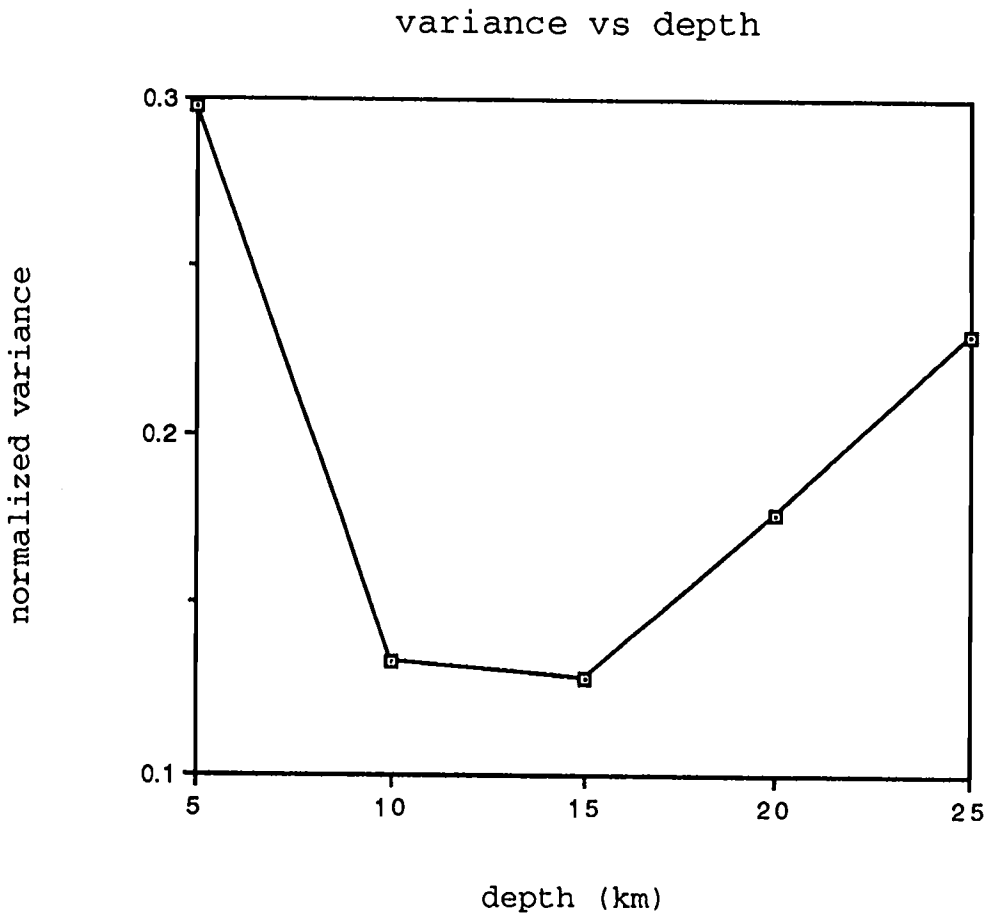

Figure 5.5 Normalized variance vs depth shows a well defined source depth between 10 and 15 km.

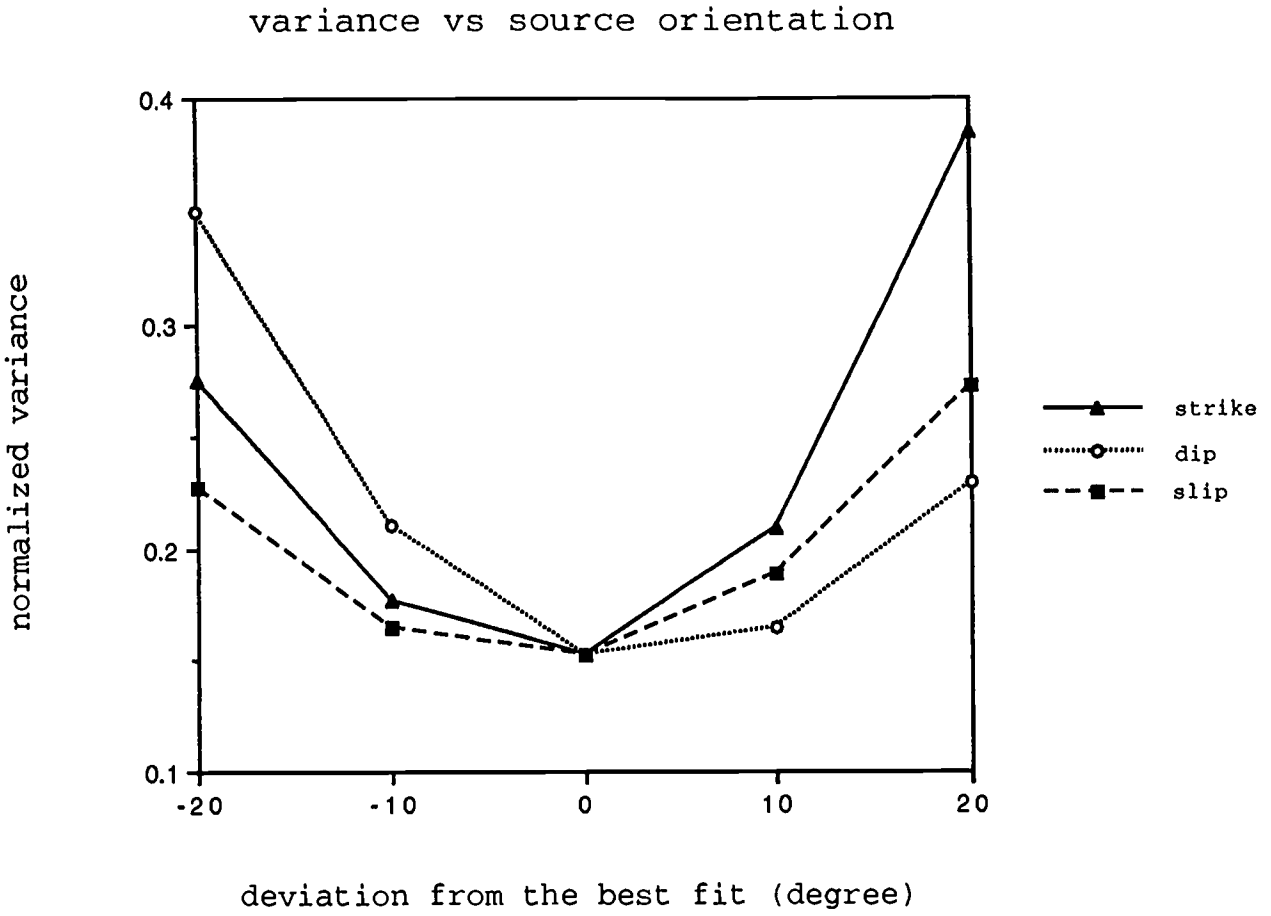

Figure 5.6 Normalized variance vs deviation from the best-fit model.

6. Inversion for two Blanco Fracture Zone Events

The Blanco Fracture Zone (BFZ) is a NW-trending transform fault between the Juan de Fuca Ridge and the Gorda Ridge. It consists of many segments of small transform faults offset by step overs.

The Blanco Fracture Zone is one of the most active regions in offshore Oregon (please refer to figure 1). Two recent medium magnitude events from the BFZ are investigated in this section.

6.1 BFZ Event I (1992)

6.1.1 Data processing

This event occurred in November 17, 1992 (m_b=4.8), and was well recorded by broadband stations COR (OSU/IRIS), LON (UofW), and WDC (U.C.Berkeley). The station information can be found in table 4. There might be some uncertainty about the instrument gain at the Longmire station. After the instrument responses were removed, the data were high-pass filtered with a cutoff frequency at 0.01 Hz and converted to ground-displacement records. The data were then resampled at a 1 second sampling interval and were all scaled to micrometers. A time window of 256 seconds is used for all three stations, and both the data and synthetics were normalized to the epicentral distance of LON (surface-wave type of normalization).

Preliminary inversion of this event shows that the origin time and epicenter were not well determined. Figure 6.1 shows the best possible waveform match in the 0.01-0.05 Hz frequency band using the origin-time and epicenter

information from the Quick Epicenter Determination (QED) catalogue. All the synthetics were computed based on QED's estimates of origin time and epicenter location; standard oceanic structure was assumed for all stations. The synthetics did not resemble the observation even for the major surface waveforms. The mislocation may be caused by the standard continental structure being used for routine epicenter determination. So I recomputed the epicentral distances and origin time based on the P to S arrival-time difference observed on the original broadband velocity records (table 4).

Deviatoric constraint is firmly applied to the moment-tensor elements, so only five moment-tensor elements plus eight triangular source time functions with 1-second half duration for each element triangular time function are to be inverted. Since most of the paths to the three stations are under the ocean, the same standard oceanic crustal structure with a 1 km thick very low velocity sediment layer on the top is used for generating synthetics at the three stations.

6.1.2 Inversion results

The inversion is performed in three different frequency bands, 0.01-0.1 Hz, 0.01-0.05 Hz and 0.01-0.03 Hz, to investigate which frequency band is most appropriate for the inversion (figure 6.2a, b and c). The match in the 0.01-0.1 Hz band is not suitable for the inversion, mainly because the dispersion behavior of the observed data are not matched at this frequency band. The inversion in the 0.01-0.1 Hz band gives a source mechanism of strike=189^0, dip=50^0, and slip=263^0, with an 84% double-couple component. Waveform matches in the 0.01-0.03 Hz and 0.01-0.05 Hz bands are comparable. In both frequency bands, the data at COR are matched fairly well. Slight phase shifts and amplitude

discrepancies are present at LON and WDC, and are more obvious in the 0.01-0.03 Hz frequency band, probably due to the oversimplified structure. The inversion in the 0.01-0.03 Hz band yields a source orientation of strike=138^0, dip=85^0, and slip=260^0, with an 81% double-couple component.

Inversion in the 0.01-0.05 Hz band gives a fault-plane solution of strike=211^0, dip=61^0 and slip=230^0, with a 94% double-couple component (figure 6.3). The seismic moment is estimated to be 8.9×10^{23} dyn cm (M_w=5.2), and the source duration is about 2 seconds. No time shifts were needed for all three stations.

Normalized variance is plotted against depth (figure 6.4), which constrains the source depth at 5 km. To have some idea about the resolution of the source orientation, the normalized variance is plotted as a function of source-orientation deviation from the best-fit model (figure 6.5). The variance has a minimum at the best slip angle, whereas the strike and dip angle are relatively poorly constrained.

This is a normal-fault solution, which suggests that this event could be one of the earthquakes that occurred on a step over.

6.2 BFZ Event II (1993)

6.2.1 Data processing

This event (m_b=5.0) occurred in May 9, 1993. Data from COR, LON, WDC, and ARC (WDC and ARC are VBB stations of the Berkeley Digital Seismic Network) are available for the analysis. The data are first high-pass filtered with a cutoff frequency at 0.02 Hz and integrated to the displacement records. The same time-window length of 256 seconds is extracted from the data, with the same 1 second

time interval; the same normalization as that in section 6.1.1 was applied to all four stations.

Firm deviatoric constraint is applied to the moment-tensor elements. If any phase shift is observed after a stable solution is reached, the seismograms are allowed to realign to maximize the cross correlation between the data and synthetics.

Again, for this event the origin time and location are not well determined. Therefore, I relocated the epicenter and origin time by picking the P and S arrivals. Since P and S arrivals are not distinct on the ARC and LON records, epicentral distance for these two stations could be inaccurate as well. These parameters are listed in table 5. The standard oceanic structure is used for all stations.

6.2.2 Inversion results

The inversions are performed in two different frequency bands, 0.03-0.1 Hz and 0.03-0.05 Hz, respectively (figure 6.6a and b). The data are quite noisy for frequencies lower than 0.03 Hz. Figure 6.7a shows the inversion of the seismograms in the 0.03-0.1 Hz frequency bnad. In this frequency band, the data have many relatively higher frequency features, which the synthetics lack. Hence, this is not an appropriate band for performing the inversion. The inversion in the 0.03-0.1 Hz band yields a source orientation of strike=119^0, dip=89^0, and slip=231^0, with a 94% double-couple component. If the high-cutoff frequency reduces to 0.05 Hz, however, the data are further smoothed. The data are well matched. The fit is not perfect, for example, a slight phase shift is observed at the transverse component of COR and the radial and vertical components of WDC; amplitudes of all three components of LON are not quite matched.

Inversion in the 0.03-0.05 Hz band gives a fault-plane solution of strike=122^0, dip=89^0, and slip=38^0, with a 98% double-couple component (figure 6.7). The seismic moment is estimated to be 2.5×10^{24} dyn cm, corresponding to M_w=5.5. The source time function is quite complicated, and has an overall duration of about 30 seconds. The time shift for ARC is +1 second, for COR +1 second, for LON -8 seconds, and for WDC -2 seconds, where a positive number means the synthetics are advanced and a negative number means the synthetics are delayed.

The normalized variance is plotted as a function of depth (figure 6.8), which shows a well defined minimum at 5 km. The strike angle has a better resolution than the dip and slip angles (figure 6.9), and the dip and slip angles are poorly constrained.

Considering the transform nature of the Blanco Fracture Zone, the solution with strike=122^0, dip=89^0, and slip=38^0 may be the real fault plane, which is essentially a strike-slip solution with a small normal left-lateral component.

Table 4. Event and station parameters for the 1992 event on the Blanco Fracture Zone.

Event parameters from the Quick Epicenter Determination (QED):

Year	Month	Day	Time	Lat (^{0})	Lon (^{0})	m_b	M_s	Depth (km)
1992	11	27	20:37:14.20	43.959	-128.365	4.8	4.4	10.0

Station parameters*:

Station	Δ(km)	Azimuth (^{0})	Instrument Type	Recomputed Δ(km)
COR	411	78.5	STS-1	499
LON	602	56.6	S-5007	701
WDC	611	126.0	STS-2	713

* The second and third columns are computed based on the QED catalogue. The recomputed origin time is 20:37:10 based on P-S intervals.

Table 5. Event and station parameters for the 1993 event on the Blanco Fracture Zone.

Event parameters from QED:

Year	Month	Day	Time	Lat(^{0})	Lon(^{0})	m_b	Depth (km)
1993	05	09	22:16:42.9	43.825	-128.039	5.0	10.0

Station parameters*:

Station	Δ(km)	Azimuth (^{0})	Instrument Type	Recomputed Δ(km)
ARC	464	133.7	STS-2	577
COR	389	75.8	STS-1	521
LON	589	54.2	S-5007	713
WDC	581	126.6	STS-2	651

* The second and third columns are computed based on the QED catalogue. The recomputed origin time is 22:16:37 based on P-S intervals.

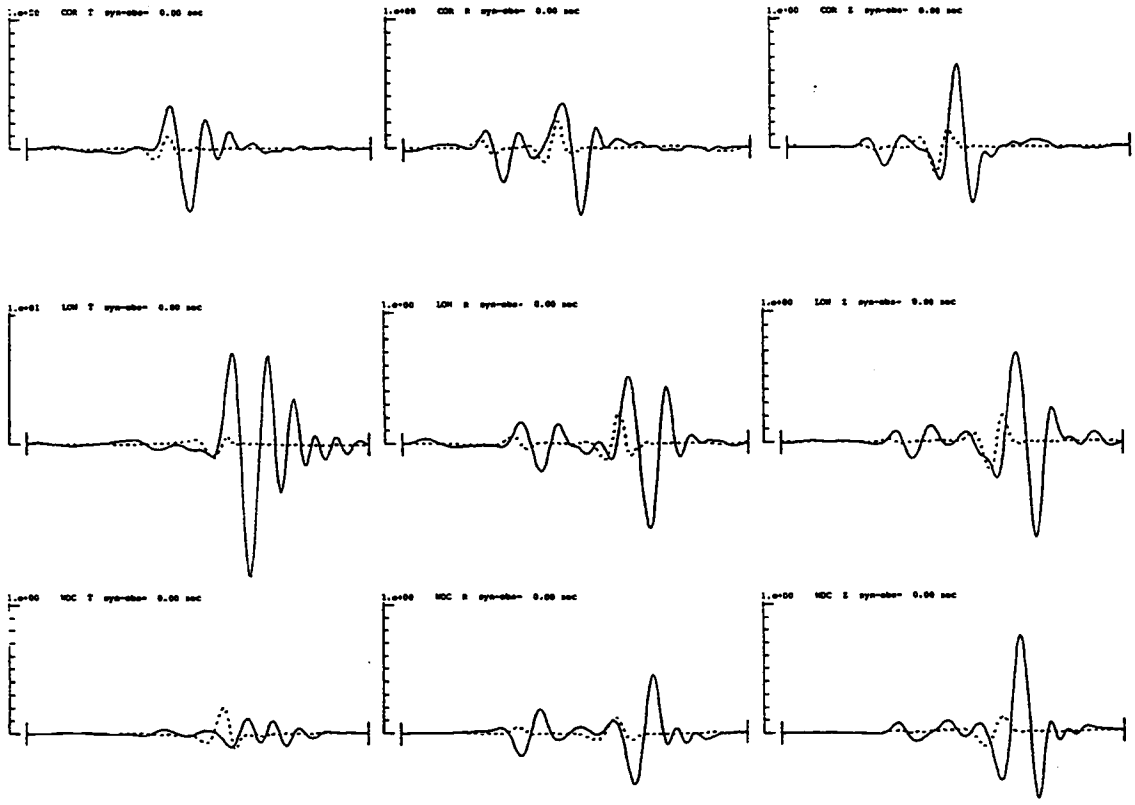

1 minute

Figure 6.1 Preliminary inversion of the seismograms for the 1992 event on the Blanco Fracture Zone in 0.01-0.05 Hz. Origin time and epicenter location are based on the QED catalogue. The solid lines are for the observed data, and dash lines for the synthetics. Stations COR (top), LON (middle) and WDC (bottom) are shown. Traces from left to right are for transverse, radial, and vertical components, respectively. The source time function is shown in the left-bottom corner.

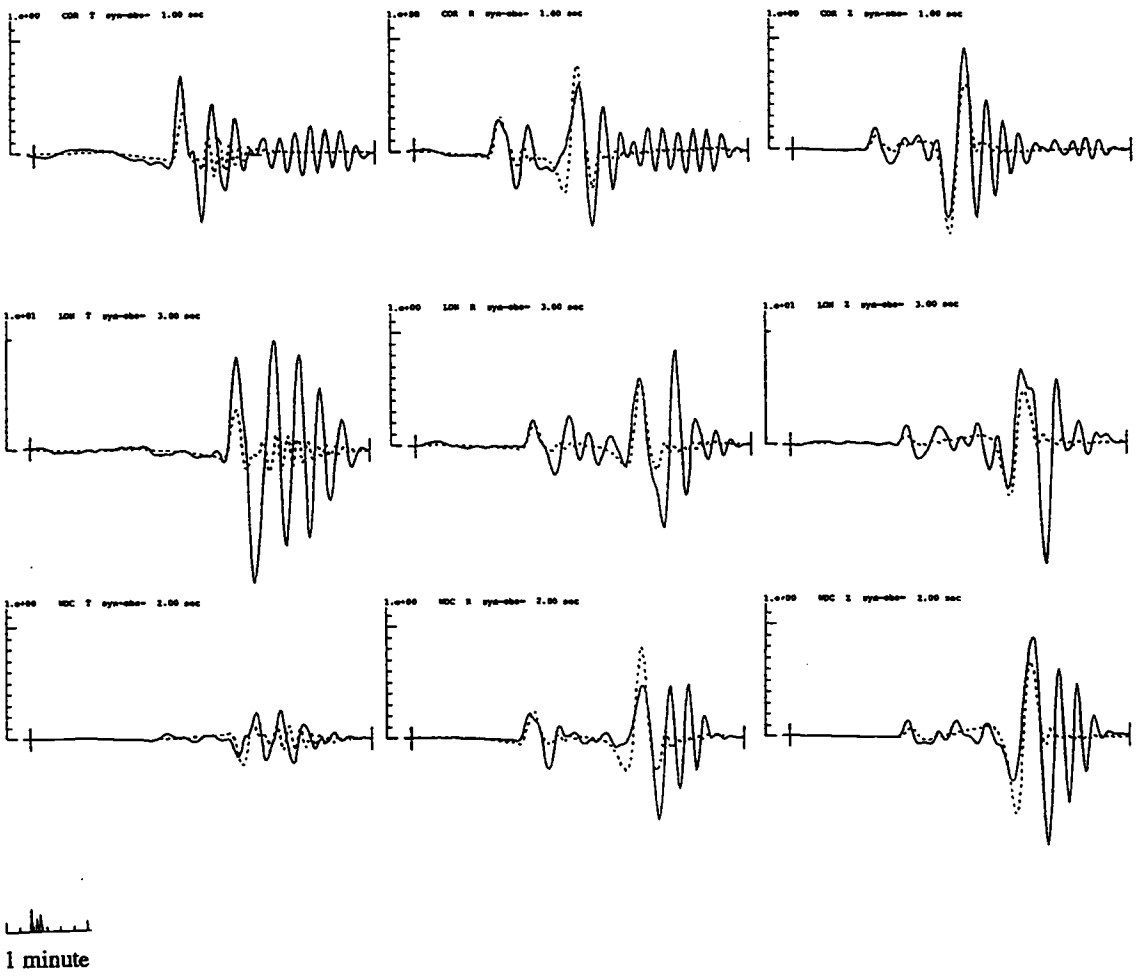

Figure 6.2a Inversion of the seismograms for the 1992 event on the Blanco Fracture Zone in 0.01 - 0.1 Hz. Origin time and epicenter distances are recomputed using P to S arrival time difference from records at the three stations.

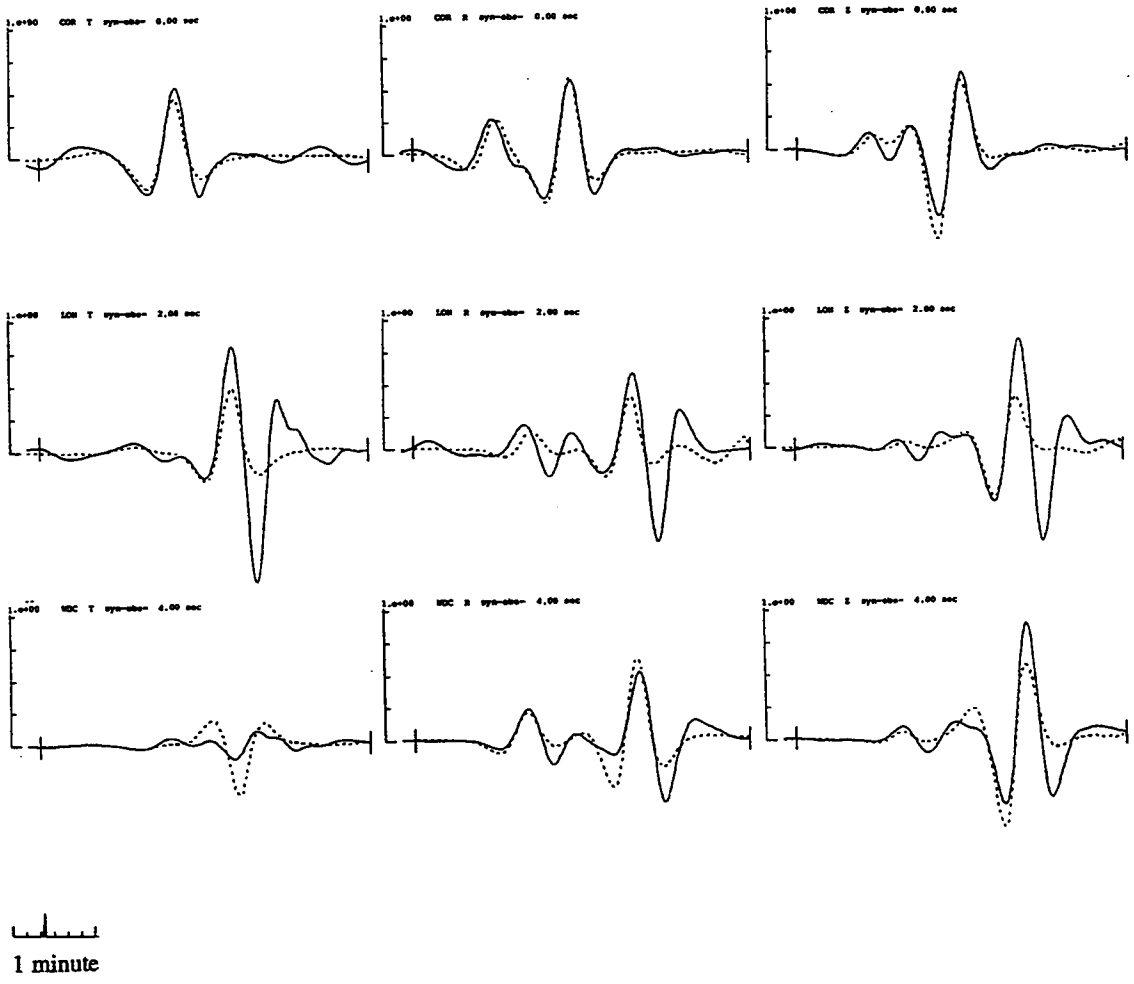

1 minute

Figure 6.2b Same as figure 6.2a, except for frequencies in 0.01-0.03 Hz.

Figure 6.2c Same as figure 6.2a except for frequencies in 0.01-0.05 Hz. This is the most appropriate frequency band used for the inversion of the 1992 event.

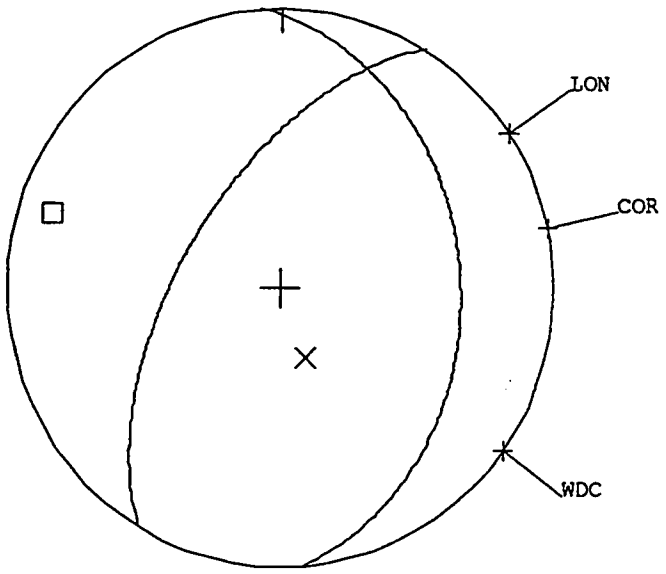

Figure 6.3 Fault-plane solution from the inversion of the seismograms for the 1992 Blanco Fracture Zone event.

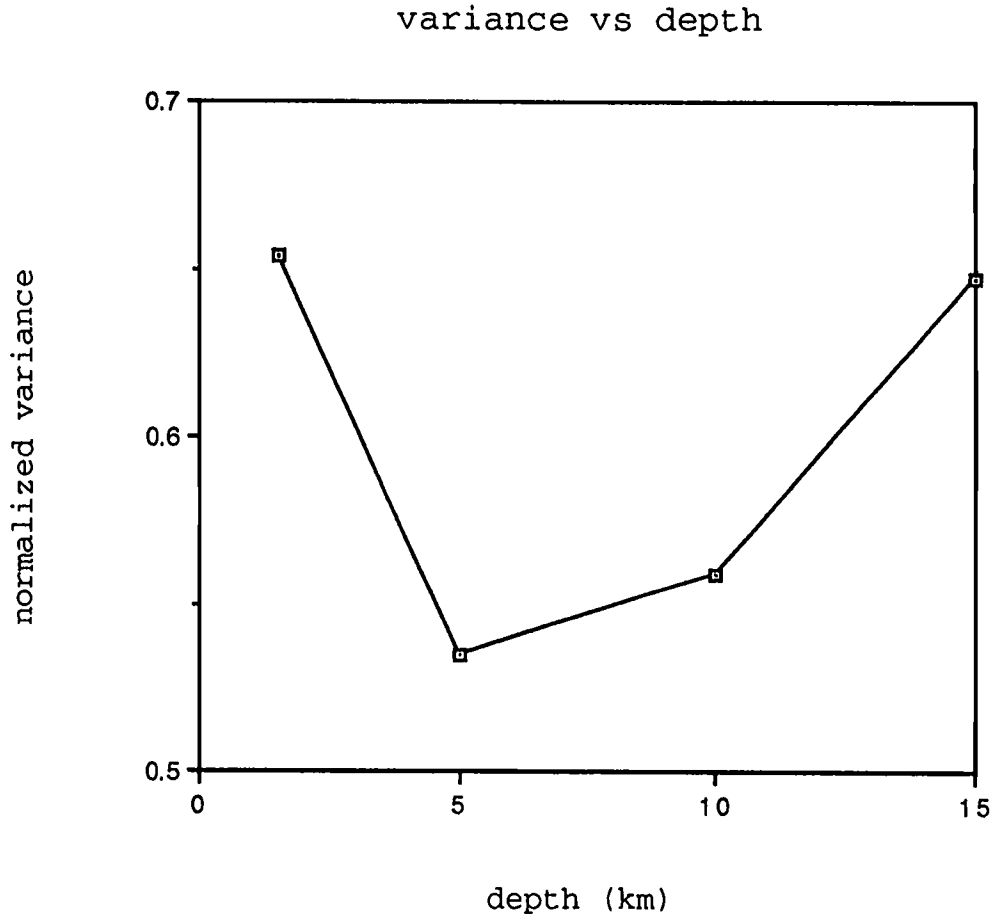

Figure 6.4 Normalized variance vs. depth plot constrains the source depth at 5 km.

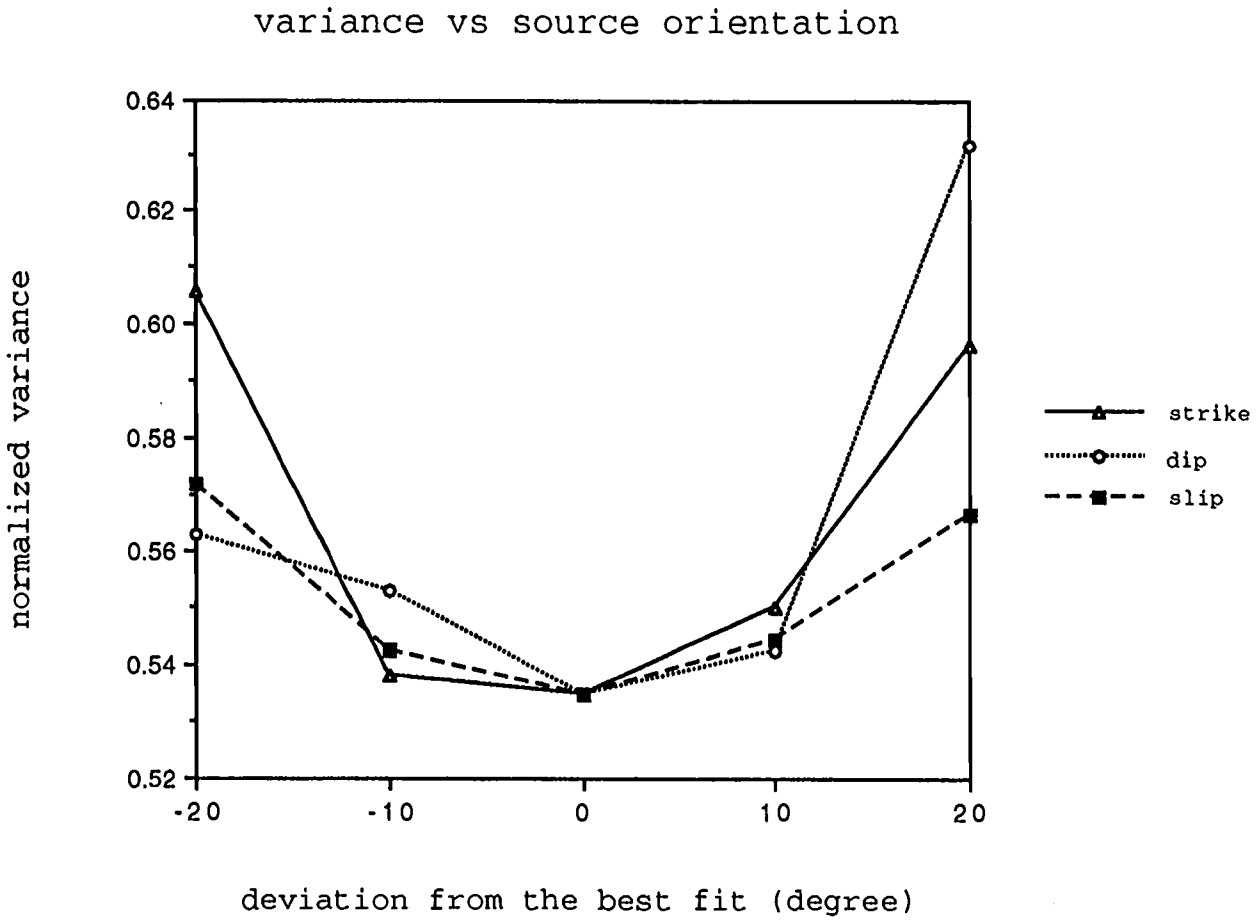

Figure 6.5 Normalized variance vs deviation from the best-fit model. The slip angle has a minimum variance at the best fit.

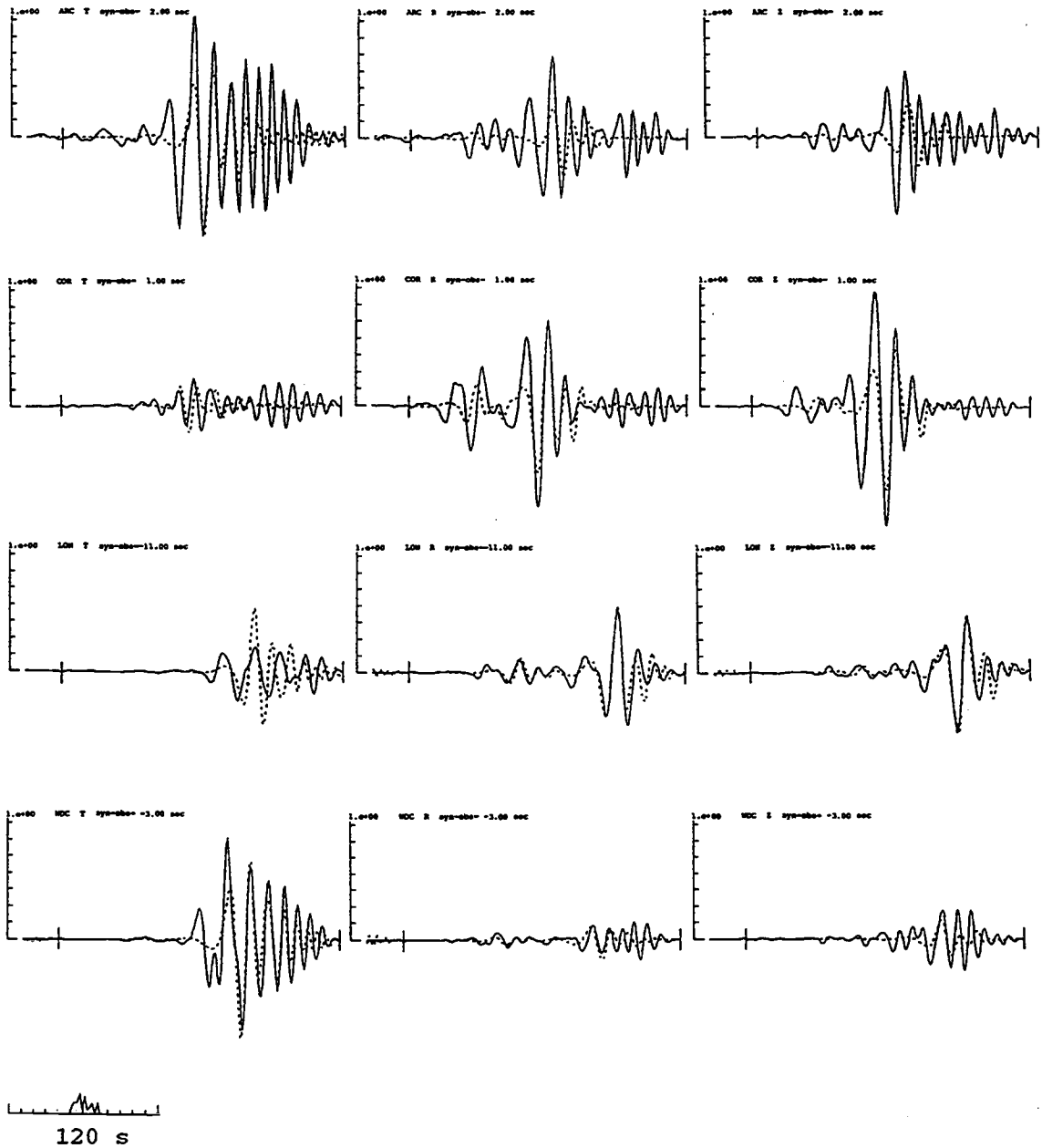

Figure 6.6a Inversion of the seismograms for the 1993 event on the Blanco Fracture Zone in 0.03- 0.1 Hz. The solid lines are for the observed data and dash lines for the synthetics. Traces from top to bottom are for stations in the order of ARC, COR, LON, and WDC, respectively. Traces from left to right are for transverse, radial, and vertical components, respectively. The source time function is shown in the left-bottom corner.

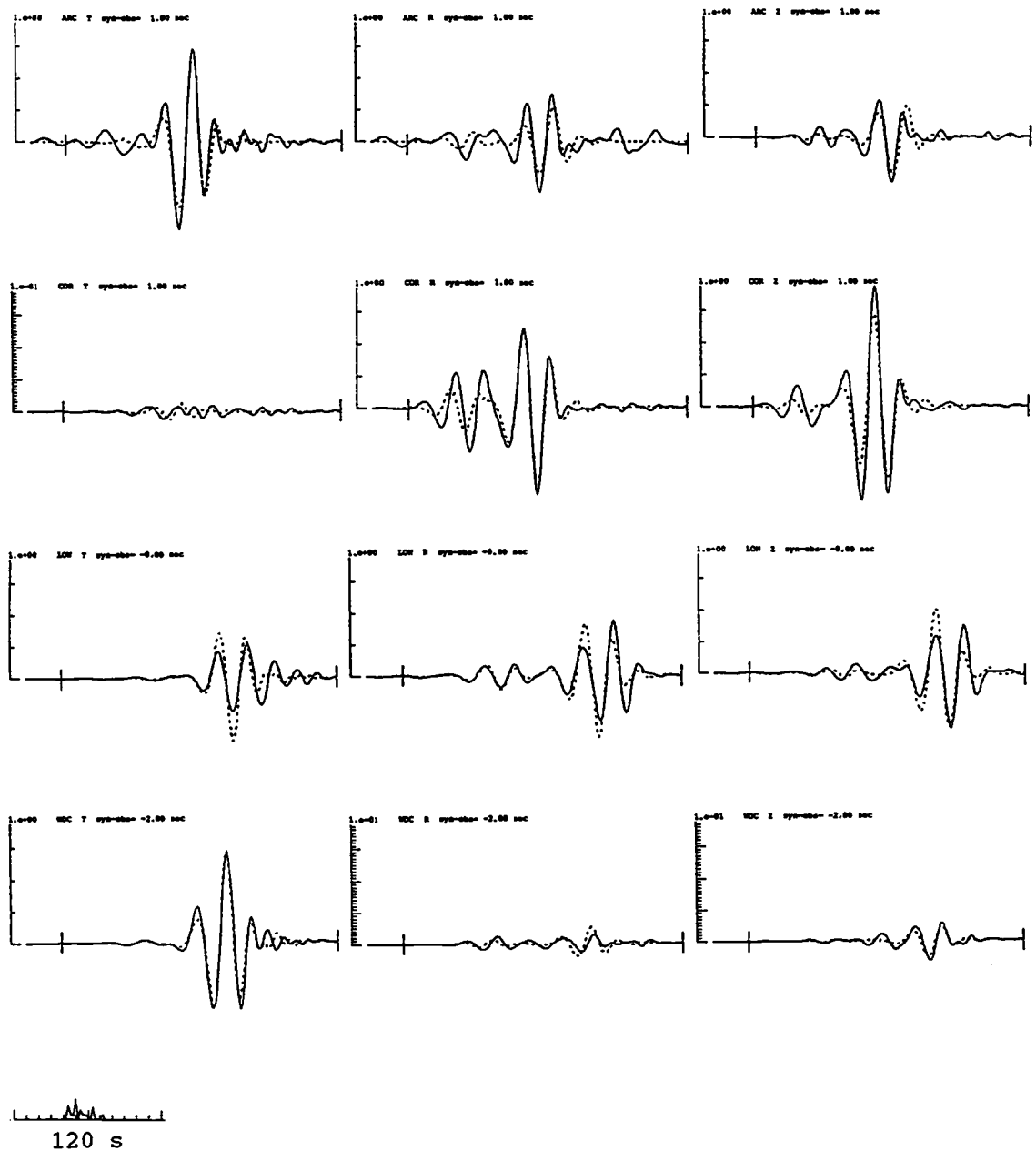

120 s

Figure 6.6b Same as figure 6.6a, except for frequencies in 0.03-0.05 Hz.

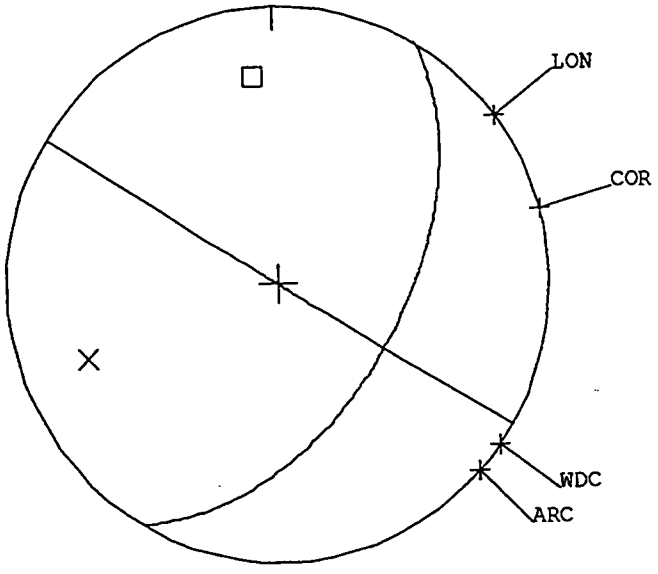

Figure 6.7 Fault-plane solution from inversion of the seismograms for the 1993 BFZ event.

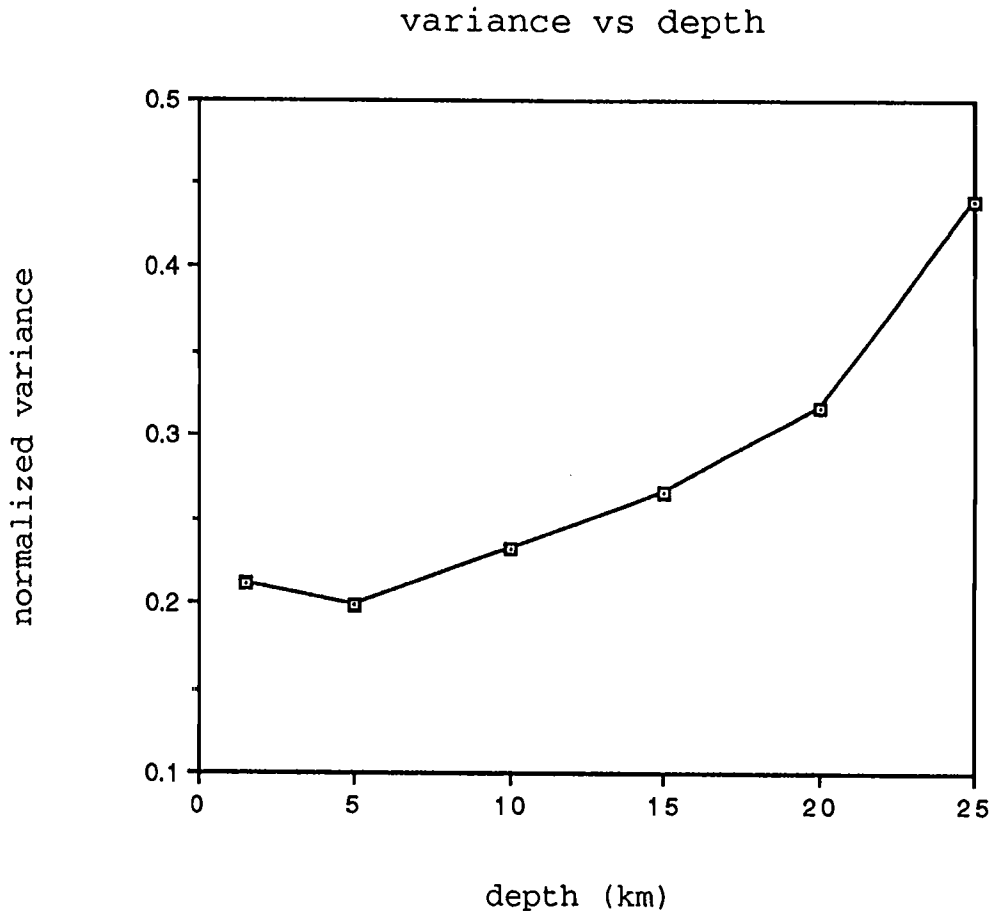

Figure 6.8 Normalized variance vs depth plot gives a well defined source depth at 5 km.

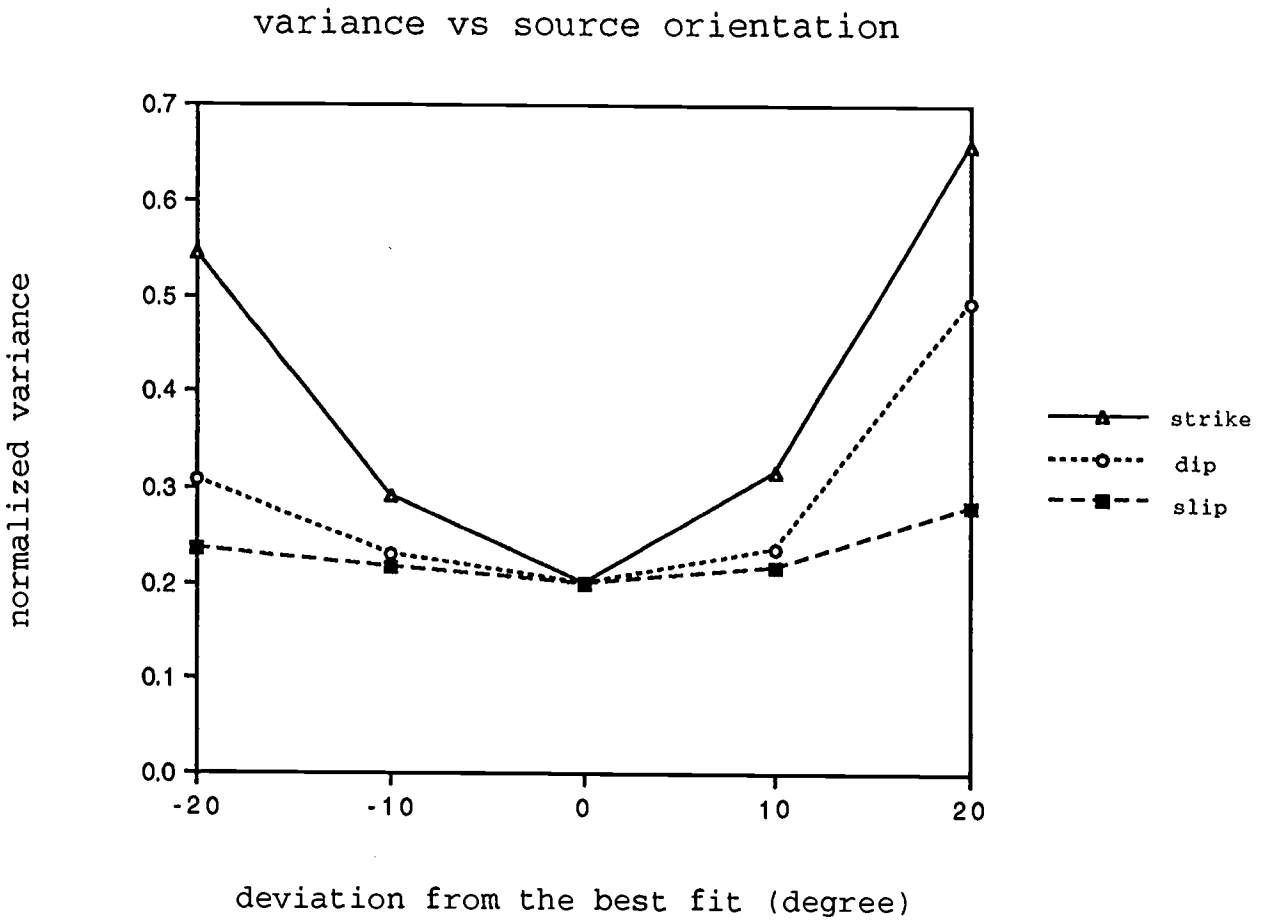

Figure 6.9 Normalized variance vs deviation from the best-fit model. Notice that the strike angle has a better resolution than the dip and slip angles.

7. Conclusions and Discussion

A moment tensor inversion method to recover source parameters for regional medium magnitude earthquakes is presented in this thesis. The code has been fully tested using a set of synthetic data. The testing shows that the inversion is efficient and flexible in retrieving source parameters. The source mechanism, seismic moment, and source depth are recovered for three basic types of source orientation: 45^0 dip-slip, vertical dip-slip, and horizontal strike-slip. The 45^0 dip-slip orientation has the best source-depth resolution, and the strike-slip has the least good resolution. The inversion is most sensitive to an adequate crustal model, especially to the upper crustal model, and also depends considerably on the accuracy of the event location. Realignment between the data and the synthetics could correct for origin time shifts and compensate for the improper crustal model and mislocation of events. In our test case, the average velocity variation cannot exceed 2.5% and the mislocation cannot exceed 5 km for frequencies lower than 0.2 Hz. Of all the source parameters, the seismic moment is most sensitive to the waveform fit, even slight phase shifts could lead to a considerably biased estimate of the seismic moment. The source mechanism, on the other hand, is relatively insensitive to a waveform misfit.

The inversion technique was applied to three medium magnitude earthquakes from both onshore and offshore Oregon. For the 1993 Scotts Mills event, using data from only two stations, the inversion gave a source mechanism that is quite consistent with the local geologic structure. The 1992 and 1993 Blanco Fracture Zone events were inverted using data from three and four stations, respectively. For these two events, the standard oceanic structure was assumed for generating excitation functions. With the relatively sparse

station distribution and very simple crustal structure, the waveform matches are reasonably good for both events.

Inasmuch as the source mechanism is relatively insensitive to the waveform misfit, we could use a relatively simple structure and invert for the seismograms at sufficiently long periods. This shows the robustness of the inversion technique. Two closely related issues concerning a good inversion arise here. First, one needs to find the appropriate frequency band for performing an inversion; secondly one needs to determine what kind of simple structure can be used for the routine processing. For the three examples shown in the thesis, the frequency bands for inversion were carefully chosen. Adequately modeled crustal structures, in other words, the Green's function, is our major concern. This is a common problem with which any regional-waveform inversion technique has to deal. In the Pacific Northwest region, several long paths, for example, from northern California, Vancouver Island, the Gorda Plate, and the Blanco Fracture Zone, can be calibrated from surface-wave studies, as by using the techniques of Taylor (1980). Better knowledge about the onshore crustal structure can be gained through many ongoing projects about the Cascadia region (for example, further results from the 1991 USGS/OSU/UTEP seismic-refraction profiles, and the 1993 OSU receiver-function experiment).

As shown in the numerical testing section, a relatively accurate event location is also important for estimating source parameters. The Washington Regional Seismic Network (WRSN) can give an epicenter location within 2 km for onshore earthquakes; but offshore events, such as events from the Blanco Fracture Zone, are poorly located, as discussed in section 6.1.1. Relocation techniques, such as the joint hypocenter determination (JHD) of Douglas (1967), may help solve this problem.

All these efforts will help to better estimate

earthquake source parameters, which in turn, will lead to our better understanding of tectonic processes and the stress field in the Pacific Northwest.

Bibliography

Aki, K., and P.G. Richard (1980). Quantitative Seismology: Theory and Methods, W.H. Freeman, San Francisco, California.

Atwater, B.F. (1987). Evidence for great Holocene earthquakes along the outer coast of Washington State, Science, 236, 942-944.

Barnard, W.D. (1978). The Washington continental slope: Quaternary tectonics and sedimentation, Marine Geology, 27, 79-114.

Braunmiller, J., T. Dahm, and K.-P. Bonjer (1993). Source Mechanism of the 1992 Roermond earthquake from surface wave inversion of regional data, submitted to Geophys. J. Int.

Bouchon, M. (1981). A simple method to calculate Green's function for elastic layered media, Bull. Seis. Soc. Am., 71, 959-971.

Bouchon, M. (1982). The complete synthesis of seismic crustal phases at regional distances, J. Geophys. Res., 87, 1735-1741.

Crosson, R.S. (1983). Review of seismicity in the Puget sound region from 1970 through 1978, in Proceedings of Workshop XIV, Earthquake Hazards of the Puget Sound Region, Washington, U.S. Geological Survey Open-File Rept. 83-19, J.C. Yount and R.S. Crosson, Editors, 6-18.

Douglas, A. (1967). Joint epicenter determination, Nature 215, 45-48.

Dreger, D.S. and D.V. Helmberger (1993). Determination of source parameters at regional distances with three-component sparse network data, J. Geophys. Res., in press.

Dziewonski, A.M., T.-A. Chou, and J.H. Woodhouse (1981). Determination of earthquake source parameters from waveform data for studies of global and regional seismicity, J. Geophys. Res., 86, 2825-2852.

Heaton, T.H. and H. Kanamori (1984). Seismic potential associated with subduction in the northwest United States, Bull. Seis. Soc. Am., 74, 933-941.

Lawson, C.L. and R.J. Hanson (1974). Solving Least Squares Problems, Prentice-Hall, Englewood Cliffs, N.J.

Li, X-Q, J.L. Nabelek and G. Zandt (1992). Geometry of subducted Juan de Fuca Plate beneath western Oregon from broadband receiver function studies, Trans. Am. Geophys. Un., 73, 391.

Ludwin, R.S., C.S. Weaver, and R.S. Crosson (1991). Seismicity of Washington and Oregon, Chapter 6, Neotectonics of North America, Decade Map Volume, D.B. Slemmons, E.R. Engdahl, D. Blackwell, D. Schwartz, and M.Zoback, editors, Geological Society of America, Boulder, Colorado, 77-98.

Madin, I.P., G.R. Priest, M.A. Mabey, S. Malone, T.S. Yelin, and D. Merier (1993). March 25, 1993, Scotts Mills earthquake--western Oregon's wake-up call, Oregon Geology, 55, 51-57, 1993.

Menke, W. (1984). Geophysical Data Analysis: Discrete Inverse Theory, Academic Press, Orlando, Florida.

Nabelek, J.L. (1984). Determination of earthquake source parameters from inversion of body waves, Ph.D. Thesis, MIT, Cambridge.

Pasyanos, M. and B. Romanowicz (1992). Inversion of regional surface waves for source parameters and structure in California, Trans. Am. Geophys. Un., 73, 372.

Randall, G.E., C.J. Ammon, T.J. Owens, and F.T. Wu (1993). Source mechanism studies using broadband regional seismograms recorded on the Tibetan Plateau, Trans. Am. Geophys. Un., 74, 207.

Romanowicz, B., and P. Guillemant (1984). An experiment in the retrieval of depth and source mechanism of large earthquakes using long period Rayleigh wave data, Bull. Seis. Soc. Am., 74, 417-437.

Taber, J.J., and S.W. Smith (1985). Seismicity and focal mechanisms associated with the subduction of the Juan de Fuca Plate beneath Washington, Bull. Seis. Soc. Am., 75, 237-249.

Taratola, A. and B. Valette (1978). Generalized nonlinear inverse problem solved using the least squares criterion, Rev. Geophys. Space Phys., 20, 219-232.

Taylor, S.R. (1980). Crust and upper mantle structure of the northwestern United States, Ph.D. Thesis, MIT, Cambridge.

Thio, H.K. and H. Kanamori (1992). Moment tensor inversions in southern California using surface waves recorded by TERRAscope, Trans. Am. Geophys. Un., 73, 376.

Trehu, A.M., J.L. Nabelek, S. Azevedo, T. Brocher, W Mooney, J. Luetgert, I. Asudah, R. Clowes, Y. Nakamura, S. Smithson, and K. Miller (1992). A crustal cross-section across the cascadia subduction zone in central Oregon, Trans. Am. Geophys. Un.,73, 391.

Uyeda, S. and H. Kanamori (1979). Back-arc opening and the mode of subduction, J. Geophys. Res., 84, 1049-1061.

Wallace, T.C., C. Ammon, T. Lay., J. Ritsema, and H. Patton (1992). Rapid source parameter retrieval at regional distance: a comparison of techniques, Trans. Am. Geophys. Un., 73, 372,

Ward, S.N. (1980). Body wave calculation using moment tensor sources in spherically symmetric, inhomogeneous media, Geophys. J. R. Astr. Soc., 60, 53-66.

Werner, K., J.L. Nabelek, R. Yeats, and S.D. Malone (1992). The Mt. Angel Fault: Implications of seismic-reflection data and the Woodburn, Oregon earthquake sequence of August 1990, Oregon Geology, 54, 112-117.

Xia, G. and J. Nabelek (1991). Crustal structure along Willamette Valley, Oregon, from broadband analysis of local earthquakes, Trans. Am. Geophys. Un., 72 , 326.

Zhao, L.S. (1993). Source estimation from broadband regional seismograms, Trans. Am. Geophys. Un., 74, 207.

APPENDIX

Appendix Manual of Moment Tensor Inversions for Regional Earthquakes (RMT)

This a a short manual describing the structure of the RMT (moment tensor inversion for regional waves) code and how to run it.

The base frame of the code is taken from bwinv84, an interactive code for inverting teleseismic body waves by Nabelek (1984). The code mainly consists of two parts: reading in the input files and excitation functions, and running the inversion.

The input files include:

1) station file (.stdt),

2) observed data (.obs),

3) crustal model used for generating synthetics (.cm).

The excitation functions can be generated within the code or outside of the code. If the excitation functions have already been stored in the current directory, the code simply reads in those excitation functions; if not, then the code will compute and store the excitation functions.

The algorithm of least-squares inversion with constraints is taken from Lawson and Hanson (1974). The resolved moment tensor was decomposed into isotropic, CLVD, and double-couple component, and the corresponding P and T axis and fault-plane solution are computed.

Input-file Preparation

Three input files need to be constructed before running the program. All three input files are formatted. The ".cm" and ".stdt" files are easy to construct. The ".obs" file should begin with

Line 1: Station code (a4) (COR, for example),

Line 2: Component code (i1) (1, 2, and 3 for transverse, radial, and vertical component, respectively),
Line 3: Number of points, starting point, ending point, event reference time, synthetic reference time
[i6,f7.4,2i6,2(2x,f2.0,f2.0,f6.2)],
Line 4: Number of zeroes and poles, number of zeroes and number of poles (3i6),
Line 5: Code of filters, low-cutoffs, high-cutoffs
[i3,2(1x,e11.3)],
Line 6: Data (5e14.6).

This format is repeated for each component of all stations.

Excitation functions are generated by the wavenumber summation technique by Bouchon (1981, 1982). We have *axitra3* and *convm3* programs on our Sparce II station, which produce three excitation functions for each station. The excitation functions are named as "$(event name).$(station label).$(excitation function label).ah". The excitation functions are conveniently labeled as "e0, e1, e2" or "i0, i1, i2".

Running RMT

One needs to go to the Tektronix 4014 emulator to run the program. The built-in manual should be sufficient to self explain how to input the initial parameters. For moment norm, one needs to put in a reasonable number (around $10^{24\pm3}$). After the first iteration, check the output on the screen. Find the singular values and the values of the model-parameters' increase. You could choose to filter the model parameters by using a damping factor slightly larger than the smaller singular values, which will help stabilize your solution. You could choose to continue iterating or to input a new set of initial model parameters. After no improvement

is obtained, you have an option to look at the waveform fits on the screen. If any further filtering or realignment is needed, you can select the entries from the main manual. Major options include choosing different time windows for inversion, realigning, applying additional filters, outputing the inversion results, screen dumping the waveforms and the fault-plane solution.

Several Reminders

I. The inversion counts on each individual point, and each component of all stations is treated independently, except for realignment, which is described in more detail in reminder II. Different weights can be applied to each component.

II. The realignment shifts the synthetic seismograms (all three components) of a given station by the same amount.

III. The unit for both observed data and synthetics is the micrometer (notice the scaling factor of 10^{19} in the code).

List of Executable Programs

1. axitra3 - computing the five elementary Green's functions in the frequency domain,

2. convm3 - computing the three excitation functions, given three $(.hist) files that include the specific source orientations responsible for the three excitation functions,

3. mtt_lsi256 - the regional-wave inversion program for 256 points of each component,

4. mtt_lsi512 - the regional-wave inversion program for 512 points of each component,

5. ah2obs - convert the .ah file to .obs file, you will be asked to input the number of points, starting and ending point of the inversion window, and filter parameters that are the same as the ones applied to the observed data.